Università degli studi di Padova
Dipartimento di Fisica “Galileo Galilei”

Emittance Measurements
in
Compact Linear Collider Test Facility

Michele Comunian

INDEX

FIGURES

1. CLIC PROJECT

1.1 Introduction

CLIC is an acronym for Compact LInear Collider.

These CERN studies concern a collider for electron-positron physics at energies beyond LEP Energy[i].

	CLIC	LEP II
Energy:	0.5 to 1 TeV c.m.	0.1 to 0.2 TeV c.m.
Luminosity:	10^{34} cm^{-2} sec^{-1}	10^{31} cm^{-2} sec^{-1}

This means one order of magnitude in energy and three orders in luminosity.

A circular machine with any reasonable radius would radiate far too much beyond about 100 GeV ($E \propto \frac{\gamma^4}{r}$) , so the solution is to go to infinite radius, i.e. a linear collider.

The goal of a linear collider study is: getting enough particle energy, high luminosity, with low power consumption and low construction costs. An obvious design aim is to make the linacs as short as possible to keep the cost down.

The beam can be accelerated by an electric field working at radio frequency in standing wave acceleration or in traveling wave acceleration.

In both the high accelerating gradients are needed to get high energies in short distances.

For examples we have[ii]:

	Working accelerating gradients	Frequency
LIL	11 MeV/m	3 GHz
SLAC	20 MeV/m	3 GHz
LEP (copper)	1.5 MeV/m	350 MHz

For CLIC we want 1 TeV of acceleration on 15 Km; this implies 80 MeV/m.

The problems with high gradients are: electrical breakdowns, field emitted currents and high power consumption (because acceleration is proportional with the electric field and the power scales with the square of the field). A possible solution for these problems is to go to high frequency, so CLIC pushes to 30 GHz, but this purchases new problems:

1. There are not power sources at so high frequency.
2. Construction and alignment tolerances become increasingly severe as size goes down, owing to beam instabilities caused by the interaction between the beam and the structures (WAKE FIELDS).

The solutions found, for these problems, are:

1 30 GHz power is generated using a drive beam which gets its energy from a superconducting drive linac power source (2 beam system)[iii].

2 The wake fields are limitated using a high repetition rate, precision active alignment for the devices[iv] and feed forward beam alignment algorithms[v].

1.2 The CLIC two beam scheme

The solution to generate the 30 GHz microwave power for the linac is to use two beams that run in parallel in two separate linacs: a microwave generating beam, (drive beam) and the accelerated physics beam (main beam)[vi]. The energy is transferred from the drive beam to the main beam via 30 GHz microwaves structures. The drive beam must be periodically re-accelerated in 350 MHz superconducting cavities to replace the energy transferred to the main beam. Both beams are relativistic and run all along the linac but:

Drive beam:
1. High current beam.
2. Relatively low energy beam (3-5 GeV).

Main beam:
1. Relatively lower current beam.
2. High energy.

So the total system is just like a transformer: current to voltage.

This scheme uses the interaction of a train of high-intensity, very short electron bunches with a traveling wave structure to generate 30 GHz rf power.

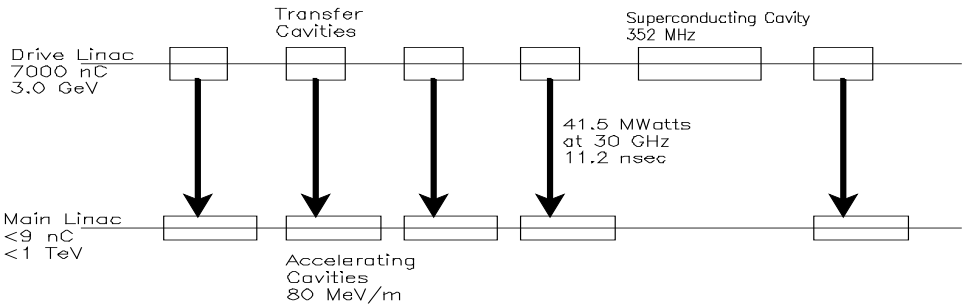

Figure 1.1 CLIC Two-beam scheme

Generation of the RF power by a drive linac rather than by thousands of individual klystrons is a distinctive feature of the CLIC design and results in a particularly simple tunnel construction.

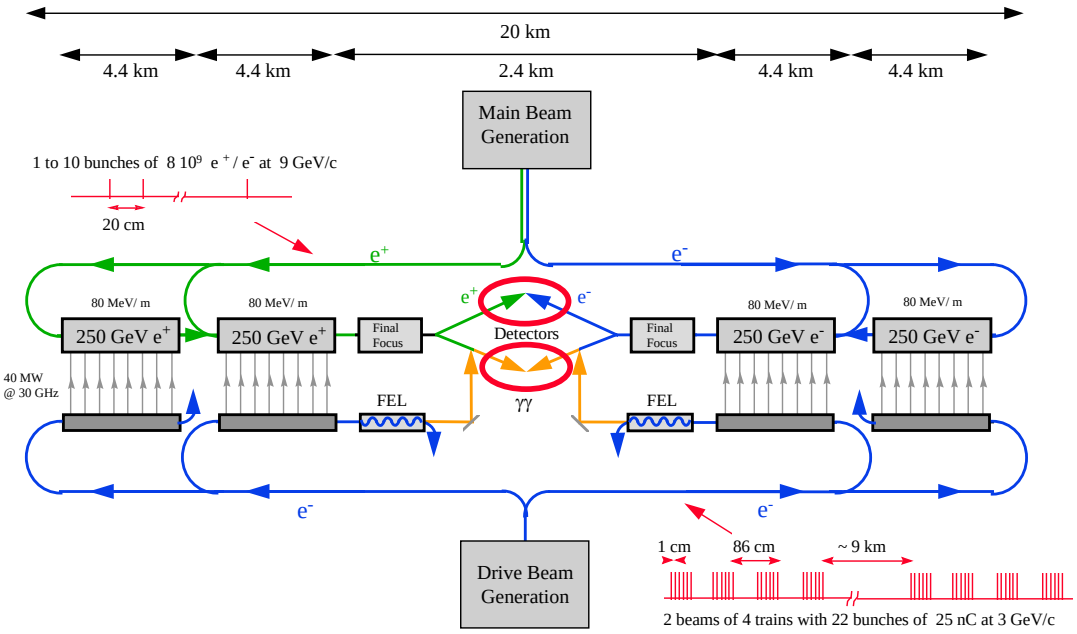

Schematic Layout of the CLIC complex at 1 TeV c.m.

Figure 1.2 CLIC schematic Layout

2. CTF PROJECT

2.1 Introduction

CTF is an acronym for CLIC Test Facility[vii].

CERN has built, and is currently operating, a test facility for linear collider studies[viii]. The aims are:

- Study the production of short, high charge electron bunches from laser illuminated photocathodes in RF guns.
- Generate high power 30 GHz RF pulses by passing bunch trains through transfer cavities for testing CLIC prototype components at nominal field levels.
- Test Beam position monitors.

The CTF is mainly composed of: (see figure 2.1[ix])

1. A 3 GHz 1.5-cell gun driven by a klystron (MDK98), equipped with a laser driven photocathode and operating at 100 MV/m. It produces a bunched beam with a momentum of 4 MeV/c and a charge of 20 nC for 8 ps FWHH-laser (35 nC for 16 ps).
2. A solenoid (SNF350) at the outlet of the gun, that provides focusing of the beam and, due to the construction, produces the higher limit in the beam size.
3. A 4-cell standing wave booster cavity driven by klystron (MDK98). It accelerates the beam to 11 MeV/c; this allows the minimisation of the space charge effects by raising the momentum.
4. A solenoid (SNF380) at the outlet of the booster. It provides some focusing of the beam; it will be substituted by a bunch compressor in 1995.
5. A 4.5 m Accelerating structure (LAS), a long travelling wave section at 3 GHz that accelerates the beam to a maximun final momentum of 90 MeV/c . It's a travelling wave diskloaded waveguide with a quasi constant gradient group velocity profile, operating in 2/3π mode. It's driven by a klystron (MDK97).
6. A beam monitor (UMA406), that measures the beam displacement and the total charge.
7. A triplet of quadrupoles (QDN410,QFN620,QDN420), used for the beam focusing.
8. A spectrometer (BHZ430) dipole, used to measure the momentum of the beam.
9. A 0.3 mm long sapphire radiator for Cerenkov radiation (CR) or a 1 mm aluminium radiator for transition radiation (TR), that can be put in the beam (TCM445). This radiation is observed with a streak camera, thus allowing to measure the time distribution as well as the transverse charge distribution of individual electron bunches. With the TR one gets a time resolution of about 2 ps (FWHH), with the CR the resolution is 3 ps. The transverse resolution of the TR is also somewhat better than that of the CR. However, the CR gives a higher signal and, contrary to the TR, it gives useful signals at low electron energies (i.e. at 4 MeV).
10. A TRS structure, that is used to extract 30 GHz RF power from the beam. It's a prototype of the CLIC accelerating structure (CAS), which is a travelling wave diskloaded waveguide of the constant impendance type, operating in 2/3π mode.

The decelerated beam, fed by the TRS, is then bent by 180° by dipole magnets at the end of the line and reaccelerated by a high gradient CLIC section (CAS).

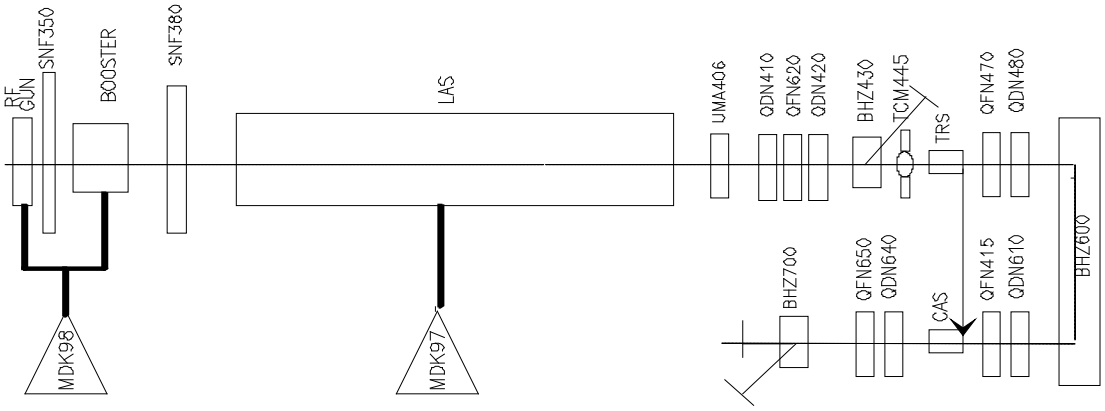

Figure 2.1 CTF Layout

3. EMITTANCE THEORY

3.1 The phase space

The equations of motion for the beam can be written in the form of Hamilton[x]:

$$\begin{cases} \dot{q}_i = +\dfrac{\partial H}{\partial p_i} \\ \dot{p}_i = -\dfrac{\partial H}{\partial q_i} \end{cases} \qquad i = 1,\ldots,r \tag{3.1}$$

Where the Hamiltonian $H(q_i(t), p_i(t), t)$ is a function of the coordinates q_i, of the conjugate moments p_i, and of the time t, the integer r being the number of degrees of freedom. If H does not explicitly depend on the time t, the Hamiltonian H is the total invariant energy of the system.

The first set of these equations allows the time derivatives $\dot{q}_i$ to be expressed in form of the conjugate moment p_i, or viceversa. The second set allows the second-order differential equations of the motion to be derived, the so-called equations of Lagrange.

The canonical phase space is the 2r-dimensional space with the conjugate coordinates q_i, p_i (i=1,...,r). The state of the system at time t is represented by a point M(t) with coordinates $q_i(t)$,$p_i(t)$ in the canonical phase space. As t increases, the representative points M(t) generate a curve, called a phase trajectory.

When the Hamiltonian is time-independent, there is only one phase trajectory originating from any point M in the phase space. Different trajectories cannot cross each other. The motion along a closed trajectory is periodic. If the phase space is two-dimensional, all trajectories originating from points inside the region limited by a closed trajectory, are bounded by this closed trajectory.

A beam of N particles is a system with 3N degrees of freedom if the internal degrees of freedom (like spin) can be neglected. The 3N coordinates q_i are the components of the coordinate vectors $\boldsymbol{r}_j$ (j=1,...,N) of each particle. The canonical phase space is 6N dimensional.

When the N particles are identical and without mutual interaction, only the canonical phase space of one particle can be considered. The latter is 6-dimensional. At time t, the state of the beam is represented by the set of N points $M_j(t)$, where the point M_j corresponds to the particle j (j=1,...,N).

The N particles form a beam only if the N points are clustered in a relatively small volume of the 6-dimensional phase space. When N is large, the beam state can be represented by its phase density $f(\vec{q},\vec{p},t)$ with $\vec{q} \equiv (q_1, q_2, q_3)$ and $\vec{p} \equiv (p_1, p_2, p_3)$ such that at time t the number dN of representative points in an infinitesimal volume $d^3p\,d^3q$ is given by:

$$dN = f(\vec{q},\vec{p},t)\,d^3q\,d^3p \tag{3.2}$$

In general, the phase density $f(\vec{q},\vec{p},t)$ explicitly depends on time t as the density does not stay constant at a fixed point $M(\vec{q},\vec{p})$.

The phase density can be considered as a probability distribution in the phase space; it can be approximated by a gaussian function, or by a uniform density in an ellipsoid.

Usually, the longitudinal motion along the beam axis is decoupled from the motion in the plane transverse to the beam axis. In that case, the 6-dimensional phase space can be split into a longitudinal phase space (2-dimensional) and a transverse phase space (4-dimensional).

Finally, if the transverse motion can be decomposed into two independent motions along two orthogonal directions, the transverse phase space can be split into two 2-dimensional phase spaces.

3.2 The Liouville's theorem

When the evolution of a physical system is governed by an Hamiltonian, the particular form of the equations of motion implies that there are quantities left invariant by the mapping.

In particular, the Liouville's theorem states that volumes in phase space are invariant.

By mapping from time t to time t', all the points $M(t)$ in a finite volume V are transformed into the points $M(t')$ that define the transformed volume V' . From the Liouville's theorem, the measures of the volume V and V' are the same. This property applies to the 6N-dimensional canonical phase space of a beam of N interacting particles, as well as to the 6-dimensional phase space of identical particles without mutual interactions. It is a property of the mapping that results from the Hamiltonian form of the equations of the motion and does not depend on the

particles themselves. In the 6-dimensional phase space, the invariance of a volume does not depend on how many particles are represented in it. There may be no particles in that volume.

Nevertheless, the hypersurface limiting a finite volume is in general not invariant.

Its geometrical form is modified, but in a such way that the enclosed volume is conserved. For instance, if *N* points, representing a beam in a 2-dimensional phase space, are enclosed in an ellipse at time *t*, then at another time *t'* , the *N* points are enclosed in a new closed curve, transformed from the ellipse and may be with a different form.

Moreover, volumes in a subspace corresponding to a part of the degrees of freedom are generally not invariant. They are invariant only when these degrees of freedom are uncoupled from the other ones. For instance, when the betatron motions are coupled, areas in horizontal and vertical phase spaces are not conserved.

An immediate consequence of the Liouville's theorem, when beam losses are negligible, is the invariance of the phase density $f(\vec{q}(t),\vec{p}(t),t)$ in the 6-dimensional phase space. More precisely, the density at the point *M(t)* is equal to the density at the transformed point *M(t')* at another time *t'*:

$$f(\vec{q}(t),\vec{p}(t),t) = f(\vec{q}(t'),\vec{p}(t'),t') \tag{3.3}$$

In other words, the phase density stays constant when running along a phase trajectory as a representative point does.

Liouville's theorem provides a powerful tool to describe a beam in phase space. Knowledge of the area occupied by particles in phase space at the beginning of a beam transport line will allow us to determine the location and distribution of the beam at any other place along the transport line without having to calculate the trajectory of every individual particle.

3.3 The beam emittance

Neglecting mutual interactions and coupling between the three coordinates of a particle, one defines the emittance of each degree of freedom; horizontal, vertical, and longitudinal.

The horizontal (vertical) emittance is defined considering the $x, x' = \frac{\partial x}{\partial s}$ phase space, instead of the x, p_x canonical phase space (s is the curvilinear abscissa along the reference orbit). One is more interested to know about the slope x' than the transverse momentum p_x.

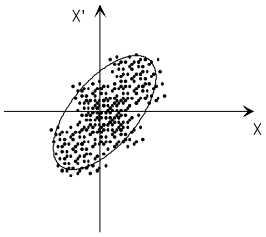

Figure 3.1 A set of points representative of a beam in the (x,x') phase space

.

It is possible to define the emittance ε_x as the area (divided by π) of the ellipse (see fig. 3.1) containing 95% of all the particles in its interior. The 95 % proportion is somewhat arbitrary: one could equally use 90 % or 99 %.

In a transport line, or in a ring without acceleration, the energy of a non-radiating particle is constant, and so is $\beta\gamma$. The Liouville's theorem states that in the *x, x' (y,y')* phase space the emittance ε_x (ε_y) is conserved. Along the line or the ring, the beam passes through focusing or defocusing lenses. The beam size Δx and the beam divergence $\Delta x'$ vary, but the emittance stay constant.

In linear or circular, accelerators, where the particle energy is varied, the emittance is not invariant. Instead, one defines the so-called normalized emittance:

$$\varepsilon_{xN} = \beta\gamma\varepsilon_x \tag{3.4}$$

that refers to the area in the x, p_x canonical phase space. The normalized emittance is conserved during acceleration.

As $\beta\gamma$ increases proportionally to the particle momentum p, the emittance ε decrease as $1/p$. It is called "adiabatic damping". An equivalent point of view is to consider that, when crossing accelerating cavities, the longitudinal momentum p_z is increased while p_x is not changed. Therefore, the slope $x'=p_x/p_z$ is decreased.

An important challenge in accelerator technology is to preserve beam emittance and even to reduce it. In spite of the Liouville's theorem, there are many phenomena that may affect the emittance. A list not necessarily exhaustive, of phenomena causing non-conservation of horizontal (vertical) beam emittance includes:

- Coupling between degrees of freedom (horizontal-vertical coupling, chromaticity...).
- Intrabeam scattering.
- Beam-beam scattering.
- Scattering of residual gas.
- Multiple scattering through a thin foil.
- Electron cooling.
- Stochastic cooling.

- Laser cooling.
- Synchrotron radiation emission.
- Filamentation due to non-linearity's.
- Wake fields.
- Space charge effects.

Some of these processes (coupling, chromaticity, filamentation,...) are Hamiltonian processes that can in principle be compensated to avoid emittance dilution.

The beam emittance can be considered as a measure of the "transverse or longitudinal temperature" of the beam and depends on the source characteristics of the beam (for example spot size).

3.4 Linear equations of motion

The distribution of focusing parameters in a beam transport system makes it impossible to formulate a general solution of the very general differential equations of motion, that come from applying the motion of charged particles in electromagnetic fields (Lorentz force) .

To describe analytically particle trajectories through a beam transport line composed of drift space, bending magnets and quadrupoles, we will derive mathematical tools which consist of partial solutions and can be used to describe complete particle trajectories.

This method makes use of the fact that the magnet strength parameters are constant at least within each individual magnet. The equations of motion become very simple since the restoring force *K* is constant and the solutions have the form of trigonometric functions. The particle trajectories may now be described by analytical functions at least within each uniform element of a transport line including magnet free drift space. These solutions can be applied to any arbitrary beam transport line, by cutting it into its smaller uniform pieces so that *K*=const. In each of this pieces we will able to follow the particle trajectories analytically through the whole transport system. This is the model generally used in particle beam optics and is called the *hard edge model*.

Using this approximation, and ignoring perturbations, the equation of motion is reduced to that of a harmonic oscillator:

$$\frac{d^2u(s)}{ds^2} + Ku(s) = 0 \quad \text{where} \quad K = const. \tag{3.5}$$

Here *u* may be used for either *x* or *y*. Any arbitrary solution *u(s)* can be expressed as a linear combination of two fundamental solutions:

$$\begin{aligned} u(s) &= C(s)u_0 + S(s)u'_0 \\ u'(s) &= C'(s)u_0 + S'(s)u'_0 \end{aligned} \tag{3.6}$$

where u_0 , u'_0 are arbitrary initial parameters of the particle trajectory and where the derivatives are taken with respect to the independent variable *s*.

The solution (3.6) of the equation of motion (3.5) may be expressed in matrix formulation:

$$\begin{pmatrix} u(s) \\ u'(s) \end{pmatrix} = \begin{pmatrix} C(s) & S(s) \\ C'(s) & S'(s) \end{pmatrix} \begin{pmatrix} u_0 \\ u'_0 \end{pmatrix} \tag{3.7}$$

In a drift space, the focusing parameter is *K*=0 and the solution of (3.6) in matrix formulation can be expressed by:

$$\begin{pmatrix} u(s) \\ u'(s) \end{pmatrix} = \begin{pmatrix} 1 & s-s_0 \\ 0 & 1 \end{pmatrix} \begin{pmatrix} u_0 \\ u'_0 \end{pmatrix} = \begin{pmatrix} 1 & l \\ 0 & 1 \end{pmatrix} \begin{pmatrix} u_0 \\ u'_0 \end{pmatrix} \tag{3.8}$$

Where $l=s-s_0$ is the length of the drift.

The amplitude *u* changes only if the trajectory has an original non vanishing slope $u'_0 \neq 0$, while the slope itself does not change at all.

For a pure quadrupole, *K* will not vanish and can be positive as well as negative. With these assumptions we solve again (3.6) and determine the integration constants by initial conditions. For *K*>0 we get the transformation for a focusing quadrupole:

$$\begin{pmatrix} u(s) \\ u'(s) \end{pmatrix} = \begin{pmatrix} \cos(\sqrt{K}L) & \frac{1}{\sqrt{K}}\sin(\sqrt{K}L) \\ -\sqrt{K}\sin(\sqrt{K}L) & \cos(\sqrt{K}L) \end{pmatrix} \begin{pmatrix} u_0 \\ u'_0 \end{pmatrix} \tag{3.9}$$

Where L is the length of focusing quadrupole.

Similarly in the other plane, with $K<0$, we get the solution for a defocusing quadrupole:

$$\begin{pmatrix} u(s) \\ u'(s) \end{pmatrix} = \begin{pmatrix} \cosh(\sqrt{-K}L) & \frac{1}{\sqrt{-K}}\sinh(\sqrt{-K}L) \\ \sqrt{-K}\sinh(\sqrt{-K}L) & \cosh(\sqrt{-K}L) \end{pmatrix} \begin{pmatrix} u_0 \\ u'_0 \end{pmatrix} \tag{3.10}$$

These transformation matrices make it straightforward to follow a particle through a transport line. Any arbitrary sequence of drift spaces, bending magnets and quadrupole magnets can be represented by a series of transformation matrices M_i . The transformation matrix for the whole composite beam line is then just equal to the product of the individual matrices. For example, the matrix M for the ten magnetic elements of fig. 3.2 is determined by the product: $M=M_{10}M_9M_8...M_3M_2M_1$

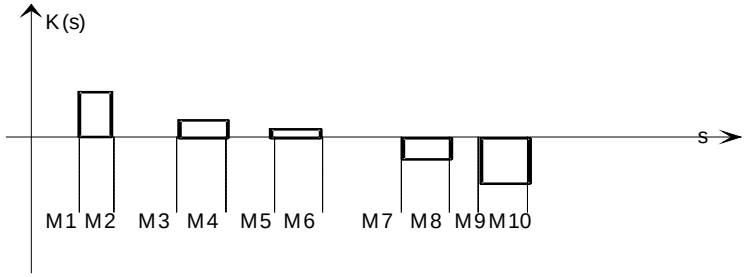

Figure 3.2 Example of a beam transport line (schematic)

and the particle trajectory transforms through the whole composite transport line as:

$$\begin{pmatrix} u(s) \\ u'(s) \end{pmatrix} = M(s|s_0) \begin{pmatrix} u_0 \\ u'_0 \end{pmatrix} \tag{3.11}$$

where $M(s|s_0)$ is the transfer matrix from the starting point s_0 (in this case is at beginning of the drift space M_1) and the end point s (at the end of the magnet M_{10}).

Because the ellipse is a quadratic form and is preserved by the line transport elements, it's easy to describe analytically an ellipse in phase space, it has become customary to surround all particle (or fraction of them) by an ellipse called the phase ellipse (see figure 3.3), for semplicity from now we use the axe x as reference instead of u.

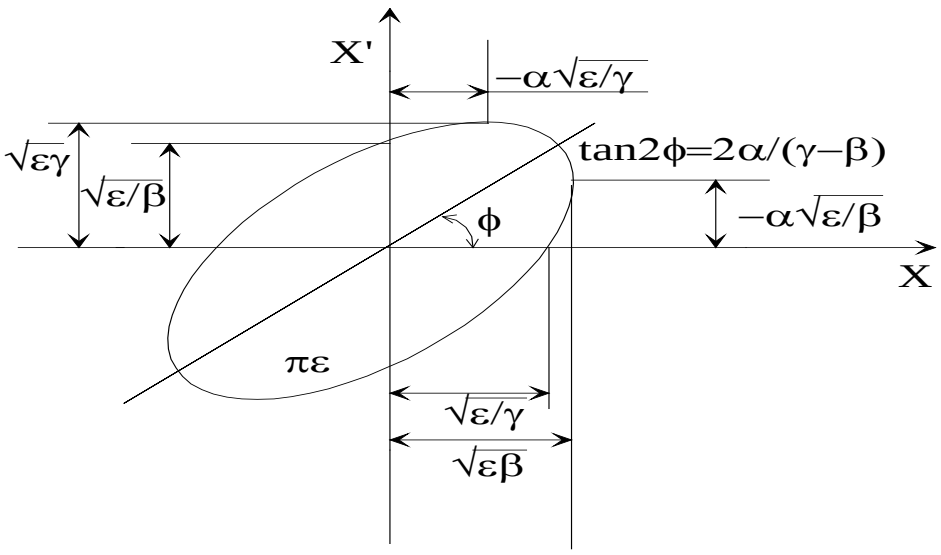

Figure 3.3 Phase space ellipse

described by:

$$\gamma\ x^2 + 2\alpha\, xx' + \beta\, x'^2 = \varepsilon \tag{3.12}$$

where α, β, γ, and ε are ellipse parameters. The area enclosed by the ellipse is called the beam emittance ε i.e.:

$$\int_{\text{ellipse}} dxdx' = \pi\varepsilon \tag{3.13}$$

while the parameters α, β and γ determine the shape and orientation of the ellipse.

The physical meaning of α is linked to the convergence or divergence of the beam. Positive values of α indicate a convergent beam and most part of the ellipse lies in the 2nd and 4th quadrant. Negative values of α mean a divergent beam with most of the ellipse in the 1st and 3rd quadrant, α=0 indicates neither convergence nor divergence and the ellipse is upsight, α is adimensional.

The square root of β is proportional to the beam envelope (by the emittance ε), so this quantity must be positive, the physical unit of β is the length (meter).

The square root of γ is proportional to the beam divergence with the same rules than β for the envelope, the unit is radiant/meter and also this quantity must be positive; in a drift space it's constant.

Since all particles enclosed by the ellipse stay within it owing to Liouville's theorem, we only need to know how the ellipse parameters transform along the beam line to be able to describe the whole particle beam. Let the equation:

$$\gamma_0 x_0^{\,2} + 2\alpha_0\, x_0 x_0' + \beta_0\, x_0'^{\,2} = \varepsilon \tag{3.14}$$

be the equation of the phase ellipse at the starting point *s*=0 of the beam line. Any particle trajectory transforms from the starting point *s*=0 to any other point s≠0 by the transformation (see 3.7):

$$\begin{pmatrix} x \\ x' \end{pmatrix} = \begin{pmatrix} C(s) & S(s) \\ C'(s) & S'(s) \end{pmatrix} \begin{pmatrix} x_0 \\ x'_0 \end{pmatrix} \tag{3.15}$$

and after solving for x_0 and x_0' and inserting into (3.14) we get after sorting coefficients:

$$\begin{aligned} &(S'^2\gamma_0 - 2S'C'\alpha_0 + C'^2\beta_0)x^2 + 2(-SS'\gamma_0 + S'C\alpha_0 + SC'\alpha_0 - CC'\beta_0)xx' + \\ &+(S^2\gamma_0 - 2SC\alpha_0 + C^2\beta_0)x'^2 = \varepsilon \end{aligned} \tag{3.16}$$

Equation (3.16) can be brought into the form (3.12) by the following substitutions:

$$\begin{cases} \gamma = S'^2\gamma_0 - 2S'C'\alpha_0 + C'^2\beta_0 \\ \alpha = -SS'\gamma_0 + (S'C + SC')\alpha_0 - CC'\beta_0 \\ \beta = S^2\gamma_0 - 2SC\alpha_0 + C^2\beta_0 \end{cases} \tag{3.17}$$

The resulting ellipse has still the same area πε as we would expect, but due to different parameters (α, β, γ), it has a different orientation and shape. During a transformation along a beam transport line the phase ellipse will therefore continuously change its form and orientation but not its area. In matrix formulation the ellipse parameters, which are also called *Twiss parameters*, transform from (3.17) as:

$$\begin{pmatrix} \beta \\ \alpha \\ \gamma \end{pmatrix} = \begin{pmatrix} C^2 & -2SC & S^2 \\ -CC' & (S'C + SC') & -SS' \\ C'^2 & -2S'C' & S'^2 \end{pmatrix} \begin{pmatrix} \beta_0 \\ \alpha_0 \\ \gamma_0 \end{pmatrix} \tag{3.18}$$

The orientation, eccentricity and area of an ellipse are defined by three parameters, while (3.14) includes four parameters α, β, γ and ε . Since the area is defined by ε we expect the other three parameters to be correlated. From geometric properties of an ellipse we find that correlation to be:

$$\beta\gamma - \alpha^2 = 1 \tag{3.19}$$

The phase ellipse in a drift space, becomes distorted in a clock wise direction without changing the slope of any particle as show in figure 3.4. The angular envelope $\sqrt{\varepsilon\gamma}$ stays constant.

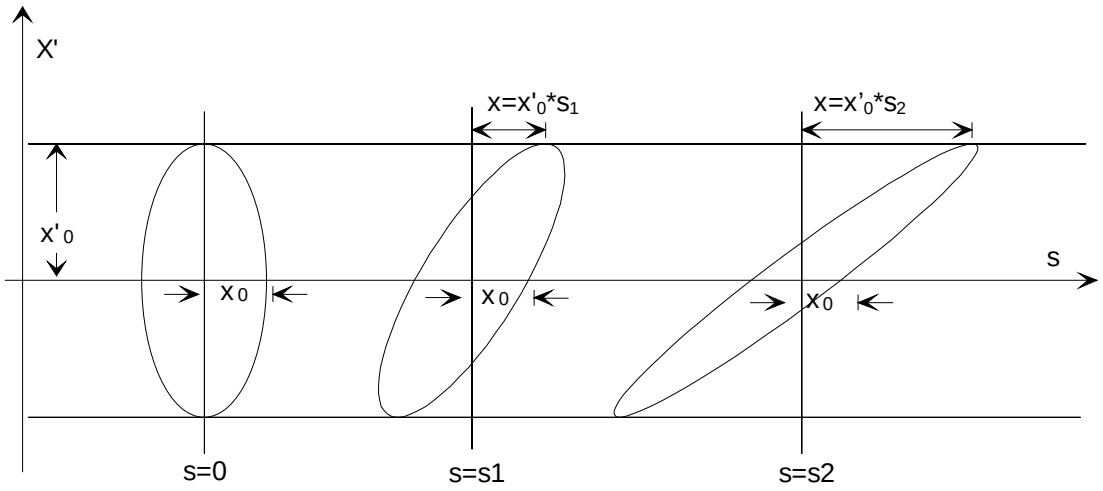

Figure 3.4 Trasformation of a phase space ellipse at different locations along a drift section

In a focusing lens, see figure 3.5, a diverging beam entering a focusing quadrupole reaches a maximum size and then starts to converge until the beam reaches its minimum called beam waist; after that the beam is transformed again into a divergent beam. But this scenario does not considerate that in the other plane the action of this quadrupole is defocusing, so you need more than one quadrupole for focusing completely the beam.

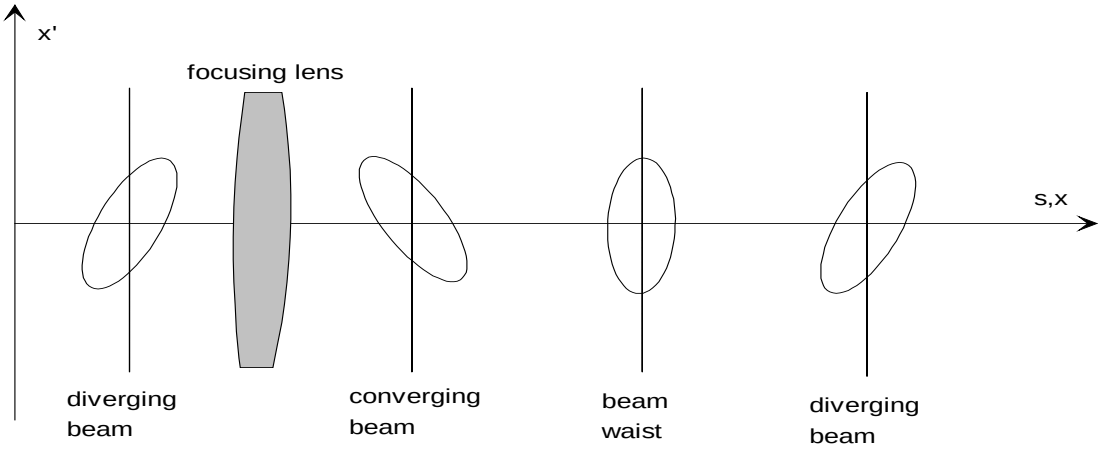

Figure 3.5 Transformation of a phase ellipse due to a focusing quadrupole

3.5 Statistical definition of beam emittance

Considering a beam as a statistically distributed set of points in a two-dimensional phase space (*x,x'*), the beam is described by the standard deviation σ_x that measures the dispersion of a set of points on a line:

$$\sigma_x = \sqrt{\frac{\sum_{i=1}^{N}(x_i - \bar{x})^2 W_i}{\sum_{i=1}^{N} W_i}} \tag{3.20}$$

where W_i is the relative "weight" of the discrete channel x_i and $\bar{x}$ is the average of the abscissa x_i of the points:

$$\bar{x} = \frac{\sum_{i=1}^{N} x_i W_i}{\sum_{i=1}^{N} W_i} \tag{3.21}$$

Similarly, the beam emittance should be a “root mean square” (r.m.s.) quantity, i.e. a function of the second-order momenta of the point distribution.

Within the statistical point of view, the emittance is not related to any contour limiting the area occupied by the points. The usual definition of emittance suffers not only from the arbitrariness of the chosen contour, but also from its distortion when time is running. It may become so twisted and bent that its area is no more representative of the spread of particles. Higher-order momenta of the point distribution could also be introduced to parametrize other aspects, like skewness, but the emittance is the main parameter of the distribution. It is possible to define the emittance ε_{rms} as the spread of the two dimensional distribution:

$$\varepsilon_{rms} = \sigma_X \sigma_{X'} \tag{3.22}$$

where σ_x and $\sigma_{x'}$ are the standard deviations in space and divergence.

This statistical definition of the emittance leads to some differences with the usual definition by means of a contour. If we interpret the two σ‘s as semi-axes of the ellipse, we have a new equation for the envelope-ellipse with area $A=\pi\varepsilon_{rms}$ respect to the axes *X, X’* :

$$\frac{X^2}{\sigma^2_X} + \frac{X'^2}{\sigma^2_{X'}} = 1 \tag{3.23}$$

For to find a more general description of the ε_{rms} we do an inverse rotation of angle -ϕ, see fig. 3.3, and we obtain its equation with respect to the new *x, x’* axes:

$$x^2\sigma^2_{x'} - 2xx' r\sigma_x\sigma_{x'} + x'^2\sigma^2_x = \varepsilon^2 \tag{3.24}$$

using the standard deviations σ_x , $\sigma_{x'}$ and the correlation coefficient *r*; with this new axes the emittance is:

$$\varepsilon_{rms} = \sigma_x\sigma_{x'}\sqrt{1-r^2} \tag{3.25}$$

That equation can also be written in the conventional form (3.12) defining the Twiss parameters such that:

$$\begin{aligned} \sigma_x &= \sqrt{\beta\varepsilon} \\ \sigma_{x'} &= \sqrt{\gamma\varepsilon} \\ r\sigma_x\sigma_{x'} &= -\alpha\varepsilon \end{aligned} \tag{3.26}$$

3.6 Particles inside an uniform and Gaussian distribution

In order to understand better the statistical definition, we want to find how many particles are inside a given ellipse defined by (3.12) if we have an analitic known distribution (3.2) i.e.:

$$\iint_{\gamma x^2 + 2\alpha xx' + \beta x'^2 = \varepsilon} f(x,x')dxdx' \tag{3.27}$$

We start with an uniform distribution, that means that inside the emittance ellipse the density is one and outside zero. This just show that the total area is given by $\pi\varepsilon_{rms}$.

We make a trasformation into polar coordinates (ρ,θ) i.e.:

$$\begin{aligned} x &= \frac{1}{\sqrt{\gamma}}\rho\cos\theta \\ x' &= \frac{1}{\sqrt{\beta}}\rho\sin\theta \end{aligned} \tag{3.28}$$

and the ellipse is transformed into:

$$\rho\left(1+\frac{2\alpha}{\sqrt{\beta\gamma}}\cos\theta\sin\theta\right)=\varepsilon \tag{3.29}$$

In this way we can solve the integral (3.27) for *f(x,x')*=1 (uniform distribution):

$$\int_0^{2\pi}\int_0^{\sqrt{\varepsilon/(1+2\alpha\cos\theta\sin\theta/\sqrt{\beta\gamma})}}\frac{\rho}{\sqrt{\beta\gamma}}d\rho d\theta=\pi\varepsilon \tag{3.30}$$

A more realistic representation of the beam distribution in phase space is the bivariante :

$$f(x,x')=\frac{1}{2\pi\sigma_x\sigma_{x'}\sqrt{1-r^2}}e^{-\frac{1}{2(1-r^2)}\left[\frac{x^2}{\sigma_x{}^2}+\frac{x'^2}{\sigma_{x'}{}^2}-\frac{2rxx'}{\sigma_x\sigma_{x'}}\right]} \tag{3.31}$$

This is the classical Gaussian distribution in two dimensions.

Using the expression (3.26) for the σ‘s and the polar coordinates (3.28) we rewrite the expression (3.31) in the form:

$$f(\rho,\theta)=\frac{1}{2\pi\varepsilon}e^{-\frac{\rho^2}{2\varepsilon}\left[1+2\frac{\alpha}{\sqrt{\beta\gamma}}\cos\theta\sin\theta\right]} \tag{3.32}$$

where we have used also the expression (3.19).

This distribution is normalized to one; this mean that it gives the probability distribution of the particles. With the double-integration in (*x*,*x'*) plane inside the ellipse (3.12) we found the fraction of the particles that lies inside our definitions of emittance, if we assume a Gaussian distribution of the beam.

This integration results:

$$\int_0^{2\pi}\int_0^{\sqrt{\varepsilon/(1+2\alpha\cos\theta\sin\theta/\sqrt{\beta\gamma})}}\frac{\rho e^{-\frac{\rho^2}{2\varepsilon}\left[1+2\frac{\alpha}{\sqrt{\beta\gamma}}\cos\theta\sin\theta\right]}}{2\pi\varepsilon\sqrt{\beta\gamma}}d\rho d\theta=1-e^{-\frac{1}{2}} \tag{3.33}$$

The result means that we take the 40% of the particles with our definition of r.m.s. emittance. In a more general way, ε_{rms} can be define by $\varepsilon_{rms}=n^2\sigma_X\sigma_{X'}$, where n is a number that gives the possibility to include more or less beam inside the ellipse; for example usually n=2 in proton machines. Now the relations (3.26) are transformed in $n\sigma_x=\sqrt{\beta\varepsilon}$, $n\sigma_{x'}=\sqrt{\gamma\varepsilon}$, $n^2r\sigma_x\sigma_{x'}=-\alpha\varepsilon$ in this way we considerate more particles inside us ellipse of area $\pi\varepsilon_{rms}$ and the results for the probability for gaussian distribution is given by:

$$\int_0^{2\pi}\int_0^{\sqrt{\varepsilon/(1+2\alpha\cos(\theta)\sin(\theta)/\sqrt{\beta\gamma})}}\frac{n^2\rho e^{-\frac{n^2\rho^2}{2\varepsilon}\left[1+2\frac{\alpha}{\sqrt{\beta\gamma}}\cos(\theta)\sin(\theta)\right]}}{2\pi\varepsilon\sqrt{\beta\gamma}}d\rho d\theta=1-e^{-\frac{n^2}{2}} \tag{3.34}$$

The plot of this probability distribution as function of *n* is given in figure 3.6.

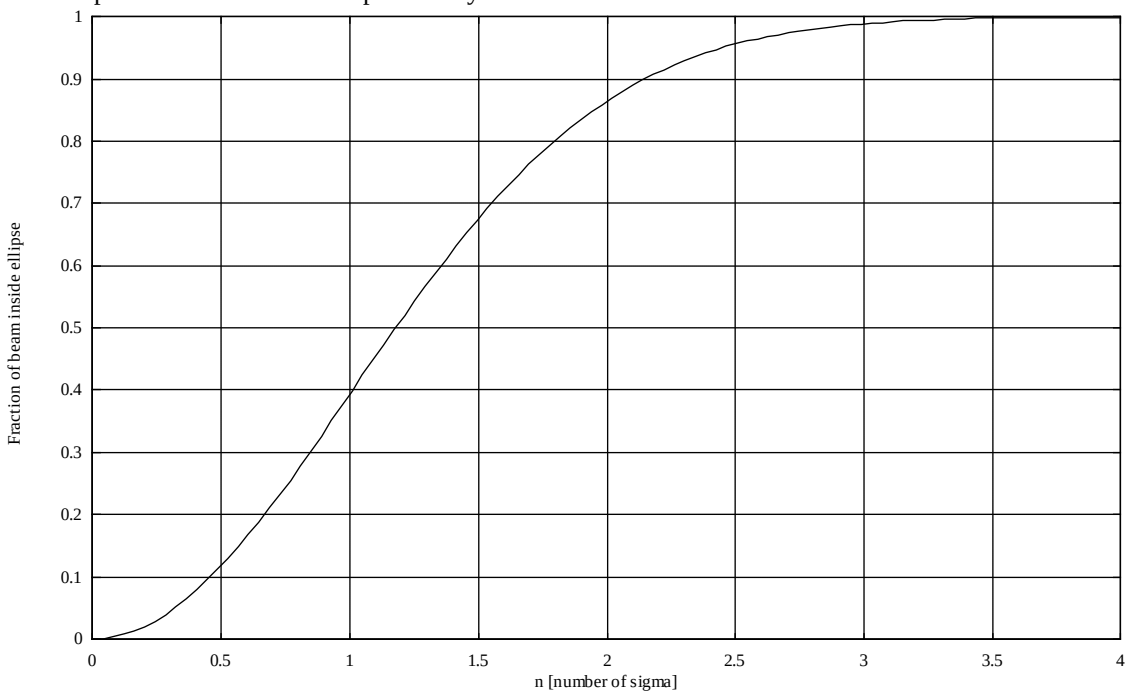

Figure 3.6 Plot of probability distribution

For example, to capturing more than 95% of the particles, the definition of emittance should be $\varepsilon_{rms} = 6\sigma_X\sigma_{X'}$.

4. METHOD TO MEASURE THE EMITTANCE IN CTF

4.1 Introduction

The ability to manipulate in a controlled and measurable way the orientation and form of the phase ellipse with quadrupoles gives us the tool to experimentally determine the emittance of a particle beam.

The beam size is measured under different focusing conditions, such that different parts of the ellipse will be probed by the beam size monitor, and the beam emittance can be determined.

To determine the emittance at point P_0 we consider, downstream P_0, a beam transport line with two quadrupoles and a beam size monitor at the place P_1. We vary the strenght of the quadrupoles and measure the beam size in P_1 as a function of quadrupoles strenght.

In figure 4.1 the part of CTF line used for this measurement is shown.

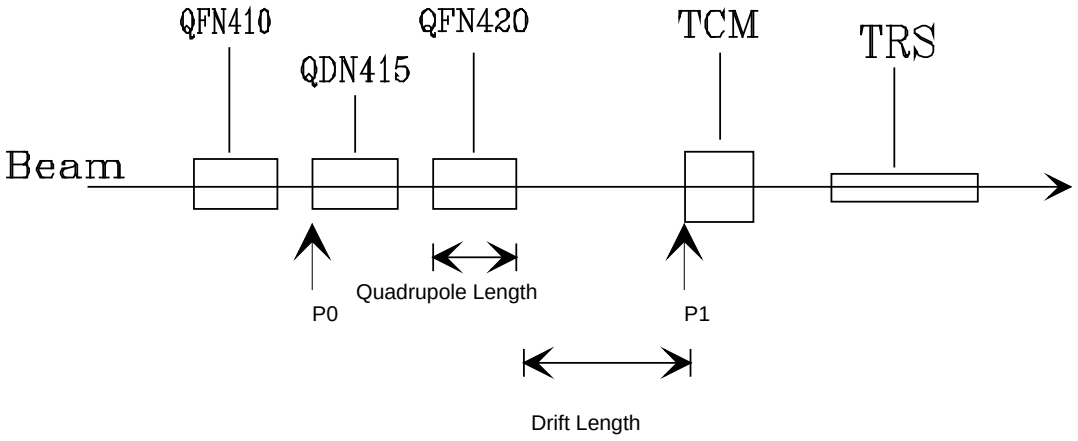

Figure 4.1 Part of CTF line used for the measurement of emittance.

4.2 Emittance calculate from three measurement of spot size

For calculating the Twiss parameters we have to take at least three measurements of beam size, because we want three parameters (α,β,γ). From the formula (3.17) we have that the beam radius is given by:

$$\begin{cases} r_1^{\,2} = C_1^{\,2}(\beta\varepsilon) - 2C_1S_1(\alpha\varepsilon) + S^2{}_1(\gamma\varepsilon) \\ r_2^{\,2} = C_2^{\,2}(\beta\varepsilon) - 2C_2S_2(\alpha\varepsilon) + S^2{}_2(\gamma\varepsilon) \\ r_3^{\,2} = C_3^{\,2}(\beta\varepsilon) - 2C_3S_3(\alpha\varepsilon) + S^2{}_3(\gamma\varepsilon) \end{cases} \tag{4.1}$$

for three differents optics: (C_1,S_1), (C_2,S_2), (C_3,S_3) of the line. These quantities are calculate by knowing the gradient of the quadrupoles and the drift lenghts with only use of the matrix theory. For having a set of independent equations, the beam must change its status from large spot size to minimal spot size to large spot size, again, with a different optics.

We have to solve the sistem (4.1) to find the Twiss parameters; for this purpose we write the system in the following way:

$$\begin{pmatrix} r_1^{\,2} \\ r_2^{\,2} \\ r_3^{\,2} \end{pmatrix} = \begin{pmatrix} C_1^{\,2} & -2C_1S_1 & S_1^{\,2} \\ C_2^{\,2} & -2C_2S_2 & S_2^{\,2} \\ C_3^{\,2} & -2C_3S_3 & S_3^{\,2} \end{pmatrix} \cdot \begin{pmatrix} \beta\varepsilon \\ \alpha\varepsilon \\ \gamma\varepsilon \end{pmatrix} \tag{4.2}$$

we call A the matrix formed by the cos-sin like elements (C_i,S_i). The inverse of matrix A is given by:

$$A^{-1} = \begin{pmatrix} \frac{S_2 S_3}{ab} & -\frac{S_1 S_3}{ac} & \frac{S_1 S_2}{bc} \\ \frac{C_3 S_2 + C_2 S_3}{2ab} & -\frac{C_3 S_1 + C_1 S_3}{2ac} & \frac{C_2 S_1 + C_1 S_2}{2bc} \\ \frac{C_2 C_3}{ab} & -\frac{C_1 C_3}{ac} & \frac{C_1 C_2}{bc} \end{pmatrix} \tag{4.3}$$

where we have call: $a = (C_1 S_2 - C_2 S_1)$ $b = (C_1 S_3 - C_3 S_1)$ $c = (C_2 S_3 - C_3 S_2)$, so the solution of sistem (4.1) is:

$$\begin{cases} \beta\varepsilon = \frac{S_2 S_3}{ab} r_1^{\,2} - \frac{S_1 S_3}{ac} r_2^{\,2} + \frac{S_1 S_2}{bc} r_3^{\,2} \\ \alpha\varepsilon = \frac{C_3 S_2 + C_2 S_3}{2ab} r_1^{\,2} - \frac{C_3 S_1 + C_1 S_3}{2ac} r_2^{\,2} + \frac{C_2 S_1 + C_1 S_2}{2bc} r_3^{\,2} \\ \gamma\varepsilon = \frac{C_2 C_3}{ab} r_1^{\,2} - \frac{C_1 C_3}{ac} r_2^{\,2} + \frac{C_1 C_2}{bc} r_3^{\,2} \end{cases} \tag{4.4}$$

These relations show how the Twiss parameters are calculated from three measurement of the beam size with an analytic procedure.

From the relation: $\beta\gamma - \alpha^2 = 1$ we have: $\varepsilon = \sqrt{(\beta\varepsilon)(\gamma\varepsilon) - (\alpha\varepsilon)^2}$ and in this way we can calculate the emittance.

Nevertheless this is not a good result because the measured radius has a statistical error that complety alterate the result obtained in this way. In an easy way we can take more than three measurement of spot size but this require a different approach for fitting the data to the theory.

4.3 The χ^2 theory

Let us assume that n measurements of the variable y_i at points x_i , are made with an error σ_i (i=1,2,...,n). It's desired to fit a function $f(x;a_1,a_2,...,a_m)$ to these data, where a_j (j=1,2,...,m) are unknown parameters to be determined. The number of points must be greater than the number of parameters (n>m). The method of least squares fit states that the best values of a_j are those for which the sum:

$$\chi^2 = \sum_{i=1}^{n} \left[\frac{y_i - f(x_i; a_j)}{\sigma_i} \right]^2 \tag{4.5}$$

is minimum[xi]. Examining (4.5) we can see that this is just the sum of the squared deviations of the data points from the curve $f(x_i)$ weighted by the respective errors on y_i.

The method is referred to as *chi-square (χ^2) minimization*. Strictly speaking this is only correct if y_i is Gaussian distributed with mean $f(x_i;a_j)$ and variance σ_i^2. However, as this is generally the case for measurements in physics, this is a valid hypotesis most of the time and also in this case. The least squares method, however, is totally general and does not require knowledge or hypotesis on the error distribution.

To find the values of a_j ,which minimize the χ^2 , one must solve the system of equations:

$$\frac{\partial \chi^2}{\partial a_j} = 0 \tag{4.6}$$

Depending on the function $f(x)$, this may or may not yield on analytic solution.

Assuming we have found the best values for a_j with this procedure, it's necessary to estimate the errors on the parameters. For this, we build the so-called covariance or error matrix, V_{ij} , :

$$(V^{-1})_{ij} = \frac{1}{2}\frac{\partial^2 \chi^2}{\partial a_i \partial a_j} \tag{4.7}$$

where the second derivatives (evaluated at the minimum) form the inverse of error matrix. The diagonal elements V_{jj} can then be shown to be the variances for a_j , while the off-diagonal elements V_{ij} represent the covariances between a_i , a_j . Thus,

$$V = \begin{pmatrix} \sigma_1^2 & \text{cov}(1,2) & \text{cov}(1,3) & \dots \\ . & \sigma_2^2 & \text{cov}(2,3) & \dots \\ . & . & \sigma_3^2 & \dots \\ . & . & . & \dots \end{pmatrix} \tag{4.8}$$

To complete the process, now, it is also necessary to have an idea of the quality of the fit. Do the data, in fact, correspond to the function *f(x)* we have assumed? This can be tested by means of the chi-square method: from theory we know that, if the data correspond to the function and the deviations are Gaussian, χ^2 should be expected to follow a chi-square distribution with mean value equal to the degrees of freedom, $\nu=n-m$, there are n independent data points ($x_1,x_2,...,x_n$) from which m ($a_1,a_2,...,a_m$) parameters are extracted. A quick and easy test is to see the reduced chi-square:

$$\frac{\chi^2}{\nu} \tag{4.9}$$

which should be close to 1 for a good fit.

4.4 Propagation of errors

When it's necessary to calculate other quantities from the fitted parameters for a given set of data, the calculated results will then contain an uncertainty which is carried over from the measured data. To see how the errors are propagated, let us consider a quantity *u=f(x,y)* where *x* and *y* are quantities having errors σ_x and σ_y , respectively. The resulting error for *u* is given by:

$$\sigma_u^2 \cong \left(\frac{\partial f}{\partial x}\right)^2 \sigma^2{}_x + \left(\frac{\partial f}{\partial y}\right)^2 \sigma^2{}_y + 2\,\mathrm{cov}(x,y)\frac{\partial f}{\partial x}\frac{\partial f}{\partial y} \tag{4.10}$$

The errors therefore are added quadratically with a modifying term due to the covariance. Depending on its sign and magnitude, the covariance can increase or decrease the errors by dramatic amounts. Some examples:

Table 4.1 Error propagation

Operation	Error
$u = x + y$	$\sigma^2{}_u = \sigma^2{}_x + \sigma^2{}_y + 2\,\mathrm{cov}(x,y)$
$u = x - y$	$\sigma^2{}_u = \sigma^2{}_x + \sigma^2{}_y - 2\,\mathrm{cov}(x,y)$
$u = xy$	$\sigma^2{}_u = y^2\sigma^2{}_x + x^2\sigma^2{}_y + 2\,\mathrm{cov}(x,y)xy$
$u = x / y$	$\sigma^2{}_u = y^{-2}\sigma^2{}_x + x^2y^{-4}\sigma^2{}_y - 2\,\mathrm{cov}(x,y)xy^{-3}$
$u = x^\alpha$	$\sigma^2{}_u = \alpha^2 x^{2\alpha-2}\sigma^2{}_x$

4.5 Beam optics for the measurement apparatus

We can consider the beam line of figure 4.1 as a quadrupole (QDN415) indicated as Lq_2 , K_2 , a drift Ld_2 , the quadrupole near the camera (QFN420) indicated as Lq_1,K_1 , and the final drift between the quadrupole and the camera Ld_1: these dynamics quantities are the lenghts and the gradients. Now we build the total transfer matrix for this line, given by multiplying all the single matrices:

$$M_{tot} = \begin{pmatrix} 1 & Ld_1 \\ 0 & 1 \end{pmatrix} \cdot \begin{pmatrix} \cos(Lq_1\sqrt{K_1}) & \frac{1}{\sqrt{K_1}}\sin(Lq_1\sqrt{K_1}) \\ -\sqrt{K_1}\sin(Lq_1\sqrt{K_1}) & \cos(Lq_1\sqrt{K_1}) \end{pmatrix} \cdot \begin{pmatrix} 1 & Ld_2 \\ 0 & 1 \end{pmatrix} \cdot \begin{pmatrix} \cosh(Lq_2\sqrt{-K_2}) & \frac{1}{\sqrt{-K_2}}\sinh(Lq_2\sqrt{-K_2}) \\ \sqrt{-K_2}\sinh(Lq_2\sqrt{-K_2}) & \cosh(Lq_2\sqrt{-K_2}) \end{pmatrix} \tag{4.11}$$

where we have supposed that the second quadrupole is defocusing in the horizontal plane (K_2<0).

The final result is the transport matrix for this line:

$$M_{tot} = \begin{pmatrix} C(K_1,K_2) & S(K_1,K_2) \\ C'(K_1,K_2) & S'(K_1,K_2) \end{pmatrix} \tag{4.12}$$

where the elements *C,S,C',S'* are given by:

$$
\begin{aligned}
C(K_1,K_2) = {} & \left[\cos(Lq_1\sqrt{K_1}) - Ld_1\sqrt{K_1}\sin(Lq_1\sqrt{K_1})\right]\cdot\left[\cosh(Lq_2\sqrt{-K_2}) + Ld_2\sqrt{-K_2}\sinh(Lq_2\sqrt{-K_2})\right] + \\
& + \sqrt{-K_2}\sinh(Lq_2\sqrt{-K_2})\cdot\left[\frac{1}{\sqrt{K_1}}\sin(Lq_1\sqrt{K_1}) + Ld_1\cos(Lq_1\sqrt{K_1})\right] \\
S(K_1,K_2) = {} & \cosh(Lq_2\sqrt{-K_2})\cdot\left[\frac{1}{\sqrt{K_1}}\sin(Lq_1\sqrt{K_1}) + Ld_1\cos(Lq_1\sqrt{K_1})\right] + \\
& + \left[\cos(Lq_1\sqrt{K_1}) - Ld_1\sqrt{K_1}\sin(Lq_1\sqrt{K_1})\right]\cdot\left[\frac{1}{\sqrt{-K_2}}\sinh(Lq_2\sqrt{-K_2}) + Ld_2\cosh(Lq_2\sqrt{-K_2})\right] \\
C'(K_1,K_2) = {} & -\sqrt{K_1}\sin(Lq_1\sqrt{K_1})\left[\cosh(Lq_2\sqrt{-K_2}) + Ld_2\sqrt{-K_2}\sinh(Lq_2\sqrt{-K_2})\right] + \\
& + \cos(Lq_1\sqrt{K_1})\sqrt{-K_2}\sinh(Lq_2\sqrt{-K_2}) \\
S'(K_1,K_2) = {} & -\sqrt{K_1}\sin(Lq_1\sqrt{K_1})\left[\frac{1}{\sqrt{-K_2}}\sinh(Lq_2\sqrt{-K_2}) + Ld_2\cosh(Lq_2\sqrt{-K_2})\right] + \\
& + \cos(Lq_1\sqrt{K_1})\cosh(Lq_2\sqrt{-K_2})
\end{aligned}
\tag{4.13}
$$

The theory that will be explained now does not depend from the exact form of the line but only from the linear relations between the coefficient *C,S,C',S'* and the Twiss parameters (3.17). We have that:

$$
r^2(K_1,K_2;\varepsilon\beta,\varepsilon\alpha,\varepsilon\gamma) = \varepsilon\beta_f = C(K_1,K_2)^2\varepsilon\beta - 2C(K_1,K_2)S(K_1,K_2)\varepsilon\alpha + S(K_1,K_2)^2\varepsilon\gamma \tag{4.14}
$$

This give the radius of the beam at the camera position as a function of the initial conditions εβ,εα,εγ of the beam and of the quadrupole gradients K_1, K_2 .

From the chi-square theory we have to minimize the quantity (4.5) and in our case we have:

$$
\chi^2 = \sum_{i=1}^{N}\frac{\left[r_i^2 - r^2(K_{1i},K_{2i};\varepsilon\beta,\varepsilon\alpha,\varepsilon\gamma)\right]^2}{\sigma^2{}_i} \tag{4.15}
$$

where σ_i^2 is the error in the square of measured ray of the beam, r_i^2 is the measured value of the beam size and N is the number of measurements done. During the process of measurement we suppose to change the quadrupole currents only in parallel form i.e. with the same number of steps (for this reason we use the same index i for both the quadrupoles) and to keep all the apparatus at the same status. So we have to search a minimal position for χ^2 by variation of $\varepsilon\beta,\varepsilon\alpha,\varepsilon\gamma$. With the use of the derivation for χ^2 we have:

$$
\begin{aligned}
0 &= 2\cdot\sum_{i=1}^{N}\frac{\left[r_i^2 - r^2(K_{1i},K_{2i};\varepsilon\beta,\varepsilon\alpha,\varepsilon\gamma)\right]}{\sigma^2{}_i}\cdot\left[\frac{\partial r^2(K_{1i},K_{2i};\varepsilon\beta,\varepsilon\alpha,\varepsilon\gamma)}{\partial(\varepsilon\beta)}\right] \\
0 &= 2\cdot\sum_{i=1}^{N}\frac{\left[r_i^2 - r^2(K_{1i},K_{2i};\varepsilon\beta,\varepsilon\alpha,\varepsilon\gamma)\right]}{\sigma^2{}_i}\cdot\left[\frac{\partial r^2(K_{1i},K_{2i};\varepsilon\beta,\varepsilon\alpha,\varepsilon\gamma)}{\partial(\varepsilon\alpha)}\right] \\
0 &= 2\cdot\sum_{i=1}^{N}\frac{\left[r_i^2 - r^2(K_{1i},K_{2i};\varepsilon\beta,\varepsilon\alpha,\varepsilon\gamma)\right]}{\sigma^2{}_i}\cdot\left[\frac{\partial r^2(K_{1i},K_{2i};\varepsilon\beta,\varepsilon\alpha,\varepsilon\gamma)}{\partial(\varepsilon\gamma)}\right]
\end{aligned}
\tag{4.16}
$$

Now we have a system of three equations in unknown $\varepsilon\beta,\varepsilon\alpha,\varepsilon\gamma$. For the derivative we obtain:

$$\frac{\partial r^2(K_{1i},K_{2i};\varepsilon\beta,\varepsilon\alpha,\varepsilon\gamma)}{\partial(\varepsilon\beta)} = C^2(K_{1i},K_{2i})$$

$$\frac{\partial r^2(K_{1i},K_{2i};\varepsilon\beta,\varepsilon\alpha,\varepsilon\gamma)}{\partial(\varepsilon\alpha)} = -2S(K_{1i},K_{2i})C(K_{1i},K_{2i}) \tag{4.17}$$

$$\frac{\partial r^2(K_{1i},K_{2i};\varepsilon\beta,\varepsilon\alpha,\varepsilon\gamma)}{\partial(\varepsilon\gamma)} = S^2(K_{1i},K_{2i})$$

and with the substitution in (4.16) we have the final form for the system (4.16):

$$\begin{pmatrix} \frac{r^2{}_i C^2{}_i}{\sigma^2{}_i} \\ \frac{r^2{}_i S_i C_i}{\sigma^2{}_i} \\ \frac{r^2{}_i S^2{}_i}{\sigma^2{}_i} \end{pmatrix} = \begin{pmatrix} \frac{C^4{}_i}{\sigma^2{}_i} & \frac{-2C^3{}_i S_i}{\sigma^2{}_i} & \frac{C^2{}_i S^2{}_i}{\sigma^2{}_i} \\ \frac{C^3{}_i S_i}{\sigma^2{}_i} & \frac{-2C^2{}_i S^2{}_i}{\sigma^2{}_i} & \frac{C_i S^3{}_i}{\sigma^2{}_i} \\ \frac{C^2{}_i S^2{}_i}{\sigma^2{}_i} & \frac{-2C_i S^3{}_i}{\sigma^2{}_i} & \frac{S^4{}_i}{\sigma^2{}_i} \end{pmatrix} \cdot \begin{pmatrix} \varepsilon\beta \\ \varepsilon\alpha \\ \varepsilon\gamma \end{pmatrix} \tag{4.18}$$

where each single term in the matrix is summed over i and $S_i \equiv S(K_{1i},K_{2i})$, $C_i \equiv C(K_{1i},K_{2i})$. After the sum, the matrix is in the form:

$$A = \begin{pmatrix} a & -2b & c \\ b & -2c & d \\ c & -2d & e \end{pmatrix} \tag{4.19}$$

where:

$$\begin{aligned} a &= \sum_{i=1}^{N} \frac{C^4{}_i}{\sigma^2{}_i} & b &= \sum_{i=1}^{N} \frac{C^3{}_i S_i}{\sigma^2{}_i} \\ c &= \sum_{i=1}^{N} \frac{C^2{}_i S^2{}_i}{\sigma^2{}_i} & d &= \sum_{i=1}^{N} \frac{C_i S^3{}_i}{\sigma^2{}_i} \quad e = \sum_{i=1}^{N} \frac{S^4{}_i}{\sigma^2{}_i} \end{aligned} \tag{4.20}$$

the determinant of A is:

$$\det(A) = -2(ace - ad^2 - b^2 e + 2bcd - c^3) \tag{4.21}$$

We know that the determinant can be different from 0 only when the number of measurements is larger than 2. The inverse of *A* is gives by:

$$A^{-1} = \frac{-2}{\det(A)} \cdot \begin{pmatrix} (ce - d^2) & -(be - cd) & (bd - c^2) \\ \frac{1}{2}(be - cd) & -\frac{1}{2}(ae - c^2) & \frac{1}{2}(ad - bc) \\ (bd - c^2) & -(ad - bc) & (ac - b^2) \end{pmatrix} \tag{4.22}$$

So, the solution of our system (4.16) is:

$$\begin{cases} \varepsilon\beta = \dfrac{-2}{\det(A)}\left[(ce-d^2)\displaystyle\sum_{i=1}^{N}\frac{r_i^2 C^2{}_i}{\sigma^2{}_i} - (be-cd)\sum_{i=1}^{N}\frac{r_i^2 S_i C_i}{\sigma^2{}_i} + (bd-c^2)\sum_{i=1}^{N}\frac{r_i^2 S_i^2}{\sigma^2{}_i}\right] \\ \varepsilon\alpha = \dfrac{-2}{\det(A)}\left[\frac{1}{2}(be-cd)\displaystyle\sum_{i=1}^{N}\frac{r_i^2 C^2{}_i}{\sigma^2{}_i} - \frac{1}{2}(ae-c^2)\sum_{i=1}^{N}\frac{r_i^2 S_i C_i}{\sigma^2{}_i} + \frac{1}{2}(ad-bc)\sum_{i=1}^{N}\frac{r_i^2 S_i^2}{\sigma^2{}_i}\right] \\ \varepsilon\gamma = \dfrac{-2}{\det(A)}\left[(bd-c^2)\displaystyle\sum_{i=1}^{N}\frac{r_i^2 C^2{}_i}{\sigma^2{}_i} - (ad-bc)\sum_{i=1}^{N}\frac{r_i^2 S_i C_i}{\sigma^2{}_i} + (ac-b^2)\sum_{i=1}^{N}\frac{r_i^2 S_i^2}{\sigma^2{}_i}\right] \end{cases} \tag{4.23}$$

What we have obtained are the values of $\varepsilon\beta, \varepsilon\alpha, \varepsilon\gamma$ that minimize the function χ^2. What we have called $\varepsilon\beta, \varepsilon\alpha, \varepsilon\gamma$ are the Twiss parameters for the system upstream the quadrupoles. Now we can calculate the errors associated with $\varepsilon\beta, \varepsilon\alpha, \varepsilon\gamma$; for this we have to calculate the covariance or error matrix V definited by (4.7):

$$V^{-1} = \frac{1}{2}\begin{pmatrix} \dfrac{\partial^2\chi^2}{\partial(\varepsilon\beta)^2} & \dfrac{\partial^2\chi^2}{\partial(\varepsilon\beta)\partial(\varepsilon\alpha)} & \dfrac{\partial^2\chi^2}{\partial(\varepsilon\beta)\partial(\varepsilon\gamma)} \\ \dfrac{\partial^2\chi^2}{\partial(\varepsilon\alpha)\partial(\varepsilon\beta)} & \dfrac{\partial^2\chi^2}{\partial(\varepsilon\alpha)^2} & \dfrac{\partial^2\chi^2}{\partial(\varepsilon\alpha)\partial(\varepsilon\gamma)} \\ \dfrac{\partial^2\chi^2}{\partial(\varepsilon\gamma)\partial(\varepsilon\beta)} & \dfrac{\partial^2\chi^2}{\partial(\varepsilon\gamma)\partial(\varepsilon\alpha)} & \dfrac{\partial^2\chi^2}{\partial(\varepsilon\gamma)^2} \end{pmatrix} \tag{4.24}$$

Note that the second derivatives form the inverse of the error matrix and this matrix form (4.8):

$$V = \begin{pmatrix} \sigma^2{}_{\varepsilon\beta} & \mathrm{cov}(\varepsilon\beta,\varepsilon\alpha) & \mathrm{cov}(\varepsilon\beta,\varepsilon\gamma) \\ \mathrm{cov}(\varepsilon\alpha,\varepsilon\beta) & \sigma^2{}_{\varepsilon\alpha} & \mathrm{cov}(\varepsilon\alpha,\varepsilon\gamma) \\ \mathrm{cov}(\varepsilon\gamma,\varepsilon\beta) & \mathrm{cov}(\varepsilon\gamma,\varepsilon\alpha) & \sigma^2{}_{\varepsilon\gamma} \end{pmatrix} \tag{4.25}$$

Now we have to calculate the second derivatives of $\chi^2(\varepsilon\beta, \varepsilon\alpha, \varepsilon\gamma)$; in our case:

$$\begin{aligned} \frac{\partial^2\chi^2}{\partial(\varepsilon\beta)^2} &= 2\cdot\sum_{i=1}^{N} -\frac{\partial r^2(K_{1i};K_{2i};\varepsilon\beta,\varepsilon\alpha,\varepsilon\gamma)}{\partial(\varepsilon\beta)}\cdot\frac{C^2{}_i}{\sigma^2{}_i} \quad = -2\sum_{i=1}^{N}\frac{C^4{}_i}{\sigma^2{}_i} \quad = -2a \\ \frac{\partial^2\chi^2}{\partial(\varepsilon\alpha)^2} &= 2\cdot\sum_{i=1}^{N} -\frac{\partial r^2(K_{1i};K_{2i};\varepsilon\beta,\varepsilon\alpha,\varepsilon\gamma)}{\partial(\varepsilon\alpha)}\cdot\frac{-2S_iC_i}{\sigma^2{}_i} = -8\sum_{i=1}^{N}\frac{S^2{}_i C^2{}_i}{\sigma^2{}_i} = -8c \\ \frac{\partial^2\chi^2}{\partial(\varepsilon\gamma)^2} &= 2\cdot\sum_{i=1}^{N} -\frac{\partial r^2(K_{1i};K_{2i};\varepsilon\beta,\varepsilon\alpha,\varepsilon\gamma)}{\partial(\varepsilon\gamma)}\cdot\frac{S^2{}_i}{\sigma^2{}_i} \quad = -2\sum_{i=1}^{N}\frac{S^4{}_i}{\sigma^2{}_i} \quad = -2e \end{aligned} \tag{4.26a}$$

$$\begin{aligned} \frac{\partial^2\chi^2}{\partial(\varepsilon\alpha)\partial(\varepsilon\beta)} &= 2\cdot\sum_{i=1}^{N} -\frac{\partial r^2(K_{1i};K_{2i};\varepsilon\beta,\varepsilon\alpha,\varepsilon\gamma)}{\partial(\varepsilon\alpha)}\cdot\frac{C^2{}_i}{\sigma^2{}_i} \quad = +4\sum_{i=1}^{N}\frac{S_iC^3{}_i}{\sigma^2{}_i} \quad = +4b \\ \frac{\partial^2\chi^2}{\partial(\varepsilon\gamma)\partial(\varepsilon\beta)} &= 2\cdot\sum_{i=1}^{N} -\frac{\partial r^2(K_{1i};K_{2i};\varepsilon\beta,\varepsilon\alpha,\varepsilon\gamma)}{\partial(\varepsilon\gamma)}\cdot\frac{C^2{}_i}{\sigma^2{}_i} \quad = -2\sum_{i=1}^{N}\frac{S^2{}_i C^2{}_i}{\sigma^2{}_i} = -2c \\ \frac{\partial^2\chi^2}{\partial(\varepsilon\gamma)\partial(\varepsilon\alpha)} &= 2\cdot\sum_{i=1}^{N} -\frac{\partial r^2(K_{1i};K_{2i};\varepsilon\beta,\varepsilon\alpha,\varepsilon\gamma)}{\partial(\varepsilon\gamma)}\cdot\frac{-2S_iC_i}{\sigma^2{}_i} = +4\sum_{i=1}^{N}\frac{S^3{}_i C_i}{\sigma^2{}_i} \quad = +4d \end{aligned} \tag{4.26b}$$

Where we have used the same notation as before for *a, b, c, d, e*. For V^{-1} we have:

$$V^{-1} = \begin{pmatrix} -a & +2b & -c \\ +2b & -4c & +2d \\ -c & +2d & -e \end{pmatrix} \tag{4.27}$$

We obtained that: $\det(V^{-1}) = -4(ace - ad^2 - b^2 e + 2bcd - c^3) = 2\det(A)$ and we can calculate the direct matrix V:

$$V = \frac{-4}{\det(V^{-1})} \cdot \begin{pmatrix} (ce - d^2) & \frac{1}{2}(be - cd) & (bd - c^2) \\ \frac{1}{2}(be - cd) & \frac{1}{4}(ae - c^2) & \frac{1}{2}(ad - bc) \\ (bd - c^2) & \frac{1}{2}(ad - bc) & (ac - b^2) \end{pmatrix} \tag{4.28}$$

So we have the errors:

$$\begin{aligned} \sigma^2{}_{\varepsilon\beta} &= \frac{-4}{\det(V^{-1})}(ce - d^2) \\ \sigma^2{}_{\varepsilon\alpha} &= \frac{-1}{\det(V^{-1})}(ae - c^2) \\ \sigma^2{}_{\varepsilon\gamma} &= \frac{-4}{\det(V^{-1})}(ac - b^2) \end{aligned} \tag{4.29a}$$

$$\begin{aligned} \mathrm{cov}(\varepsilon\beta, \varepsilon\alpha) &= \frac{-2}{\det(V^{-1})}(be - cd) \\ \mathrm{cov}(\varepsilon\beta, \varepsilon\gamma) &= \frac{-4}{\det(V^{-1})}(bd - c^2) \\ \mathrm{cov}(\varepsilon\alpha, \varepsilon\gamma) &= \frac{-2}{\det(V^{-1})}(ad - bc) \end{aligned} \tag{4.29b}$$

From the theory of the errors, to calculate the error associated with the emittance, we have to consider the propagation of errors. By definition of Twiss parameters we have that $\beta\gamma - \alpha^2 = 1$ and by multiplication of both sides by ε^2 we have:

$$\varepsilon^2 = (\varepsilon\beta)(\varepsilon\gamma) - (\varepsilon\alpha)^2 \tag{4.30}$$

with errors:

$$\begin{aligned} \sigma^2{}_{(\varepsilon\beta)(\varepsilon\gamma)} &= (\varepsilon\beta)^2 \sigma^2{}_{(\varepsilon\gamma)} + (\varepsilon\gamma)^2 \sigma^2{}_{(\varepsilon\beta)} + 2\,\mathrm{cov}(\varepsilon\beta, \varepsilon\gamma)(\varepsilon\beta)(\varepsilon\gamma) \\ \sigma^2{}_{(\varepsilon\alpha)(\varepsilon\alpha)} &= 4(\varepsilon\alpha)^2 \sigma^2{}_{(\varepsilon\alpha)} \\ \sigma^2{}_{\varepsilon^2} &= \sigma^2{}_{(\varepsilon\beta)(\varepsilon\gamma)} + \sigma^2{}_{(\varepsilon\alpha)(\varepsilon\alpha)} \end{aligned} \tag{4.31}$$

For the emittance we have from Table 4.1 (last row, α=1/2):

$$\begin{aligned} \varepsilon &= \sqrt{\varepsilon^2} \\ \sigma^2{}_{\varepsilon} &= \frac{1}{4\varepsilon^2}\sigma^2{}_{\varepsilon^2} \end{aligned} \tag{4.32}$$

Therefore the statistical error of the measured emittance is given by:

$$\sigma^2{}_{\varepsilon} = \frac{\beta^2(b^2 - ac) + \gamma^2(d^2 - ce) + 2\beta\gamma(c^2 - bd) + \alpha^2(c^2 - ae)}{\det(V^{-1})} \tag{4.33}$$

5. EXPERIMENTAL APPARATUS

5.1 System configuration

The CTF runs with electron bunches at typically several nC of charge and a bunch lenght of less than 10 ps FWHH[xii]. The CTF electron beam is produced by a photocathode excited by a high-density laser beam. It's accelerated by a cavity in the gun itself to about 4 MeV, and then by another accelerating structure to 90 MeV. The electron beam is converted into a photon beam with a similar distribution. The converter (TCM) is based on transition radiation or Cherenkov radiation phenomena[xiii].

The observation of the photon distribution in the horizontal, vertical and longitudinal plane is done by a streak camera based system.

The photon beam is transported to the streak camera by lenses and mirrors. It can be seen that:

- Cherenkov radiation is produced by relativistic particles ($\gamma>2$): the Cherenkov effect requires the speed of the electron to be higher than the speed of the photon in the glass. This explains the limit $\gamma>2$ to use this phenomenon;
- Transition radiation is produced for any electron energy but the efficiency is about 100 times smaller than Cherenkov radiation if $\gamma<100$.

As the energy of the electron beam in the CTF is between $\gamma=9$ and $\gamma=100$ it appears that Cherenkov radiation is the more efficient conversion type, but the time resolution which can be achieved by transition conversion is better and this conversion type is also more accurate for the transverse bunch dimension measurement. So we decided to use the transition radiation method for the emittance measurements[xiv].

Table 5.1 Simulation and experimental data in CTF (1993-1994):

Element	Units	Simulation (Parmela)	Experimental result
Laser pulse at the gun			
Spot size	σ_{ro} (mm)	3	
	Total (mm)	12	10
Duration	σ_{to} (ps)	3.8	
	FWHH (ps)	9	9
Photo cathode			
Emitted charge	Q_0 (nC)	10	10
RF gun			
Max. Cathode E field	E_0 (MV/m)	100	100
Initial phase	ϕ_0 (deg)	45	20-50
RF power	P_{rf} (MW)	5.85	6
Booster			
Electric field on axis	E (MV/m)	70	70
Phase	Φ (deg)	90	90
bunch at the TRS			
Momentum	p (MeV/c)	81.8	80
Energy dispersion	σ_E (%)	0.4	< 0.2
Length	σ_z (mm)	1.0	1.1
	FWHH (ps)	8	9
Transverse size	σ_x (mm)	0.2	0.5
	σ_y (mm)	0.4	0.5
Divergence	Q_f (nC)	1.2	-----
Charge		2.8	2.8

5.2 TCM

In the CTF machine the electron beam is measured at about 4 MeV ($\gamma=9$) and 90 MeV ($\gamma=180$). The useful light bandwidth for the TCM is 400-600 nm.

Table 5.2 Transition Cherenkov comparison

	Units	Cherenkov		Transition	
Electron energy	γ	9	100	9	100
Receiver aperture θ_r	mrad	190	13	190	13
Conversion efficiency[1)]	photon/electron	2.4	30	10^{-2}	1.4
Emittance (4σ) x/x_e		1	1	1	1
y/y_e		0.4	0.46	1	1
x'	rad	6	1.2	0.5	$4*10^{-2}$
y'	rad	1.2	$7*10^{-2}$	0.5	$4*10^{-2}$
		0.9			
Time dispersion (if $y_e<0.1$ mm)	ps	1.4	1.4	$2*10^{-3}$	10^{-3}

[1)] The conversion efficiency is the number of photons produced by one electron in the unit solid angle: $\Delta N/n_e \Delta x'_r \Delta y'_r$.

From table 5.2 appears that the Cherenkov converter is between 20 to 240 times more efficient in photon density production, depending on the electron energy, and that the transition converter is less time dispersive and gives less vertical error.

In order to observe the total distribution of electrons in each bunch, in the longitudinal and in the transverse planes, the system contains three parts:

1. The converter station (TCM) (transition Cherenkov monitor) and its vicinity, which converts the electron beam to a photon beam. It has three stades: the Cherenkov converter placed in the electron beam; the two converters outside the beam. There are several stations along the electron beam pipe where the electron energy is from 4 MeV to 90 MeV.
2. The streak camera, which measures the time or the transverse distribution of the photon beam. It has three works setting: the "real time mode" which displays the time distribution of the photon beam; the "transverse mode" which displays the transverse distribution of the beam, and also the horizontal and the vertical profiles; the "combined mode" which displays the transverse distribution of each bunch.
3. The optics, which transports the photon beam from the converter to the streak camera, includes three parts: the particular optics adapted to the station position along the pipe; the common optics, which collects all the photon beams produced by a different station and adapts the streak camera acceptance to the photon beams; the rotating mirror which connects the chosen station to the common optics like a periscope[[xv]].

5.3 The Streak Camera

The streak camera includes a slit (around 50 μm to 3 mm variable width, and 6 mm height) which reduces the vertical dimension of the measured photon beam to improve the time resolution of the system. An image of the slit is made on the photocathode, which converts photons to electrons. These electrons are accelerated and, if desired, deflected proportionally to time (in "real-time mode") as in an oscilloscope. The electron beam is multiplied by a microchannel plate and converted into a photon beam by a phosphor lamina. This beam is observed by a CCD camera so that the time-distribution of the input photon beam is converted to a space-distributed photon beam. The *y* axis is a combined function of longitudinal (or time) and vertical distribution; the *x* axis is a function of the horizontal distribution. The streak camera presents the following technical characteristics:

- Acceptance: x=6 mm

  y=50 μm-3 mm

  y'=x'=0.16 rad
- Time dispersion: Δt=2 ps FWHM in the 290 ps full-scale range.
- Time range: from 290 ps full scale up to 32 ns.
- Sensitivity: In the visible bandwidth the noise is equivalent to 60 photons per ps, on the faster sweeping time range (290 ps full scale). The spectrum sensitivity goes from 200 to 750 nm.

The streak camera can be used in three modes:

1. *The transverse mode (or video mode)*: the electron beam is not deflected, which allows one to see the input photon beam in the transversal plane as is done by a CCD camera. The width of the slit is maximized to increase the vertical space aperture. This mode is used for the emittance measurement.

2. *The longitudinal mode (or real-time mode)*: the electron beam is deflected to measure the time distribution of the electron beam. The width of the slit is minimized. The streak camera is triggered like an oscilloscope.

3. *The combined mode (or real-time video mode)*: the electron beam is deflected as in the longitudinal mode and the width of the slit is just as the beam size. The transversal distribution of each bunch is displayed.

The system to analyze the image of the streak camera (see fig. 5.1) is formed by a digital CCD camera, a card AVP for the acquisition of the image running in a PC with the AT bus and a program ANIMATER that displays and analyze the image. The camera is equipped by a capture CCD image integral formed of 576 lines with 384 points (THOMSON TH7883), the video gain is 8 and the analogic-digital converter (8 bits) is installed inside the camera.

The overall system performance depends on the streak camera mode used.

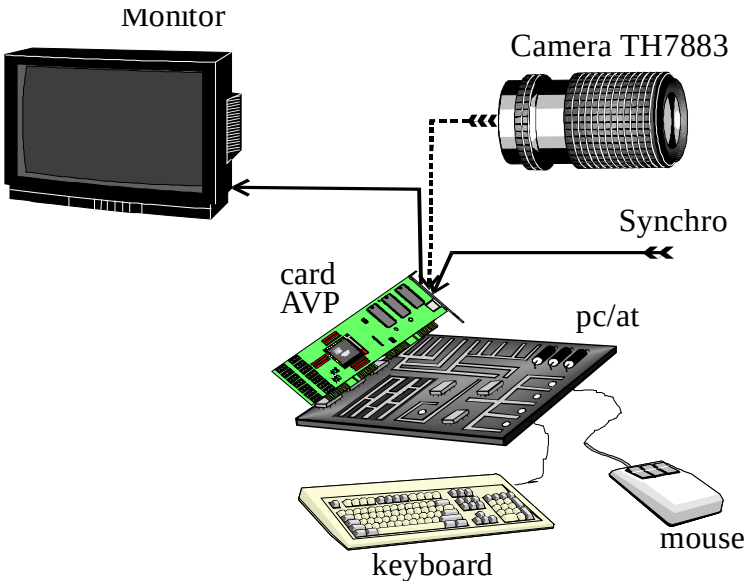

Figure 5.1 Layout of the Streak-Camera

Table 5.3 Streak camera modes

	TCM 205,340		TCM 445,435	
	Cherenkov	Transition	Cherenkov	Transition
Electron energy (MeV)	4	4	50	50
Photon wavelength (nm)	400-600	400-600	400-600	400-600
Longitudinal mode				
Intensity resolution[1)] (electrons/ps*mm)	$2*10^4$	$5*10^6$	$4*10^4$	$8*10^5$
Dynamic range	100	100	100	100
static range	1000	1000	1000	1000
Time resolution[2)] (FWHM ps)	3	2.2	3	2
Time range (full scale ns)	0.29-32	0.29-32	0.29-32	0.29-32
Time linearity	5%	5%	5%	5%
Time absolute precision (full scale)	1%	1%	1%	1%

	TCM 205,340		TCM 445,435	
	Cherenkov	Transition	Cherenkov	Transition
Transverse mode				
Intensity resolution[3)] (electrons/mm)	10^4	$2*10^6$	$2*10^4$	$3*10^5$
Dynamic range	100	100	100	100
Static range	1000	1000	1000	1000
Space resolution (mm) Vertical Horizontal	0.2 0.1	0.1 0.1	0.1 0.1	0.1 0.1
Space range (mm) Vertical Horizontal	2.4 3	1.2 3	15 15	10 24

[1)]Noise equivalent value on the 290 ps range.
[2)]For the 290 ps range; more generally the resolution is about 1% of the full scale.
[3)]Noise equivalent value.

5.4 Quadrupoles

The quadrupoles QFN410,QDN420 and QFN620 are identical to the QL1 type quadrupoles used on LIL[xvi] .

They are arranged in triplet configuration.

Table 5.4 Parameters of QDN420-QFN620

Quantity	QDN420	QFN620
Effective length	223.5 mm	223.5 mm
Mechanical length of iron stack	200 mm	200 mm
Inscribed circle radius	29 mm	29 mm
Magnetic gradient	B'[T/m]=0.2506*I[A]	B'[T/m]=-0.056*I[A]
Focal length	*f*[m]=0.05956*P[MeV/c]/I[A]	*f*[m]=0.05956*P[MeV/c]/I[A]
Max. allowed current	15 A	15 A
Max. magn. Gradient	3.76 T/m	0.84 T/m

6. AUTOMATIC SYSTEM OF MEASUREMENT OF EMITTANCE

6.1 Introduction

The variable quadrupoles method, described in 4.2, was used for the CTF because its simplicity and versatility. In figure 6.1 it's showed how the system works: the electron beam hits the TCM and a photon beam is produced, that goes into a streak camera, from the PC connected to the camera the beam profile is calculated in one plane, and the results are written in a file on the network. This file is read by the program EASY[xvii] (Emittance with an Automatic SYstem), running in an other PC, that calculates the second momentum of the profile (σ) and its size FWHH and stores the results. This program also controls, by network, the quadrupoles QDN420 and QFN620, in this way it's possible to read the actual value of quadrupole gradients and to set a new value. At this point the program EASY puts a new value of current in the quadrupoles, after 10 seconds, necessary for to set the quadrupoles, a new profile of the beam is taken by the streak camera and this is a new point for the curve beam size Vs. current in the quadrupoles.

After a complete scan around the waist of the beam, the program EASY repeats again all this procedure to calculate the errors associated with this measurement, usually after four complete scans the program starts the procedure of fitting to calculate the emittance, that is shown immediately after finishing the measurement process.

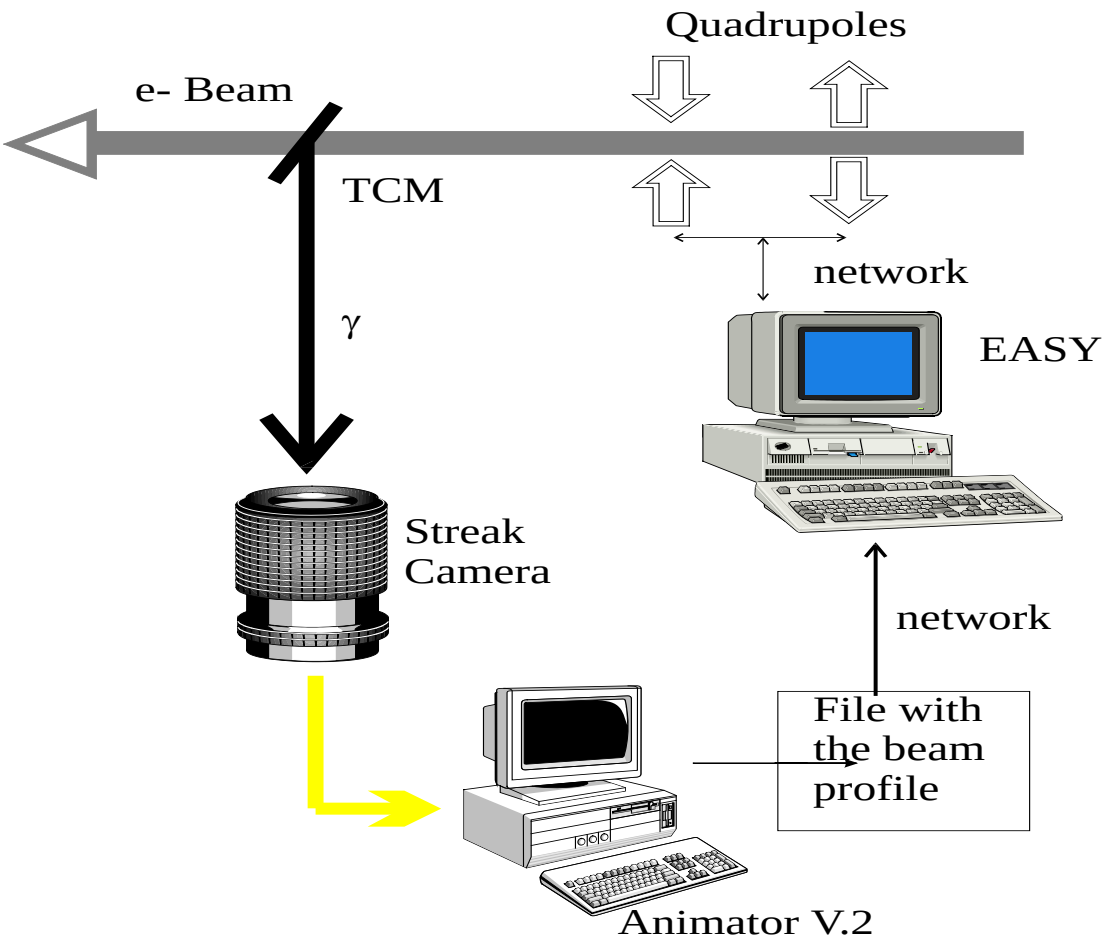

Figure 6.1 Setup for emittance measurement

6.2 Streak Camera set-up for the measurement of the emittance

The camera is working in "transverse mode", as described in 5.2, to have the horizontal and vertical profiles, when we have only one bunch, and in "time mode" when we have more than one bunch, in this case we can take only the horizontal profile because the vertical one shows the time distribution of the beam.

During the measurement, the program Animator-V2 is put in loop to store in automatic way one profile every 10 seconds.

This program reads the streak camera values of the beam imagine directly by a computer card, and calculate the beam profiles, in a automatic way.

6.3 Quadrupole set-up during the measurement

Before starting the measurement, we have to look for a quadrupole setting which gives a beam waist in the TCM. Around this point we do the measurement by choosing an interval like large spot, smallest spot, again large one.

This procedure is done in manual way. The minimum, and maximum values of the quadrupole currents and the total number of measurements selected are stored in the program EASY. We change the quadrupoles currents proportionally i.e. with the same number of steps for both, from the minimum to the maximum. The goal for the quadrupole setting is to have an almost circular shape of the beam during the measurements, to avoid the problem of cutting part of the beam if it is too large in some direction.

6.4 General beam set-up

During the measurement we want to keep all the conditions in the machine constant, therefore it's necessary to minimize the total time of the measure because it's more difficult to keep stable conditions for a long time.

The charge of the beam is adjusted by putting attenuators in the laser before it hits the photocathode. The spot size can also be changed by an iris in front of the laser, so we can do measurements with different spot sizes.

Before of the measurement of the emittance, the momentum of the beam is measured by a spectrometer and the value is stored in the program EASY.

6.5 Time needed for the measurement

The total time needed for an emittance measurement is mainly determined by the time necessary for setting the quadrupoles and for taking the profiles.

In figure 6.2 it is showed the flow chart of the principal software (EASY) used to obtain the emittance in an automatic way. The time during the measurement is so formed:

Table 6.1 Time of the measurement process

Process	Time
Setting the quadrupoles	4 seconds
Delay	5 seconds
Take the profile of the beam	10 seconds
Calculations	<< 1 second

The total time is delayed by 5 seconds because we want to be sure that the values read are coming after having set the new values in the quadrupoles; this time of 20 seconds is for taking one point in the diagram beam size versus quadrupole current. Thus the total time t_M (in seconds) of one emittance measurement is given by:

$$t_M = N_p * N_{mea} * 20 \qquad (6.1)$$

where N_p is the number of points that we want for the curve and N_{mea} is the number of times we repeat the procedure to have the error estimations. A typical measurement of emittance, with N_p=10 points for the fitting and N_{mea}=4 sets of measure, requires a total time of 10*4*20=800 seconds (~15 minutes).

6.6 Calculations done in the measure process

From the beam profile we compute the second momentum distribution (RMS) by using the formulae (3.20) and (3.21) with W_i being the weight of the channel coming from the streak camera file (an integer number from 0 to 131072=512*256) and x_i the position of the channel (from 0 to 512). This integer numbers, coming from the analogic-digital converter of the camera, are transformed in physical units by the calibration factor, typically 20 pixel/mm, so we have a resolution of 0.05 mm. When the measurement is ended the results are used in the fitting routine described by the formulae (4.19) with the errors calculated by the formulae (4.31) and the emittance is calculated by the formula (4.32).

The program EASY also calculates the FWHH of the beam profile by using a routine that finds the width of the curve of the profile at half of its maximum by two linear fits at its slope. In this way also the emittance FWHH is calculated.

The optics used in the program for the fitting routines is very general: just two drifts and two quadrupoles that can be used for any combinations of values (i.e DOFO or FOFO or FODO or FO and so on..).

The errors on the beam width measurement are calculated by repeating the measurement several times and taking the average value of the second momentum distribution of the profile and the $\sigma_{\bar{r}^2}{}^2$ defined by the formula:

$$\sigma_{\bar{r}^2}{}^2 = \frac{1}{N_{mea}-1}\sum_{i=1}^{N_{mea}}(r_i^2 - \bar{r}^2)^2 \tag{6.2}$$

where r_i^2 is the root mean square value of the profile.

We made also an estimation of the systematic error due to the error on the beam momentum measurement (± 3%) by repeating the fitting three times: with the nominal value of the momentum in the optics, with +3% in momentum and with -3% in momentum.

In this way we obtained three values of emittance and we can consider the systematic error ($\sigma_{\varepsilon S}$) to be given by:

$$\sigma_{\varepsilon S} = \frac{\left(\left|\varepsilon_+ - \varepsilon\right| + \left|\varepsilon_- - \varepsilon\right|\right)}{2} \tag{6.3}$$

The statistical errors can be reduced by doing a lot of measurements (increasing N_{mea}) but the systematic error remains the same. For this reason we chose to repeat the measurements only four times: the total time stays low and the two errors are in the same order of magnitude. The same error routines are used for the calculation of the FWHH emittance. We observed that the FWHH measurement of the profile has usually a higher statistical error than the RMS measurement.

6.7 Measurement process

For the emittance measurement we must select a value of charge of the electron beam and the spot size of the laser beam; these are the principal parameters of the measurement. The beam optics (solenoids, booster, gun phase) is also important for the measurement, but they are free parameters, in the sense that it's always possible to measure the emittance for all the values that we take for these parameters. In figure 6.2 it's reported the flow chart of the measurement process.

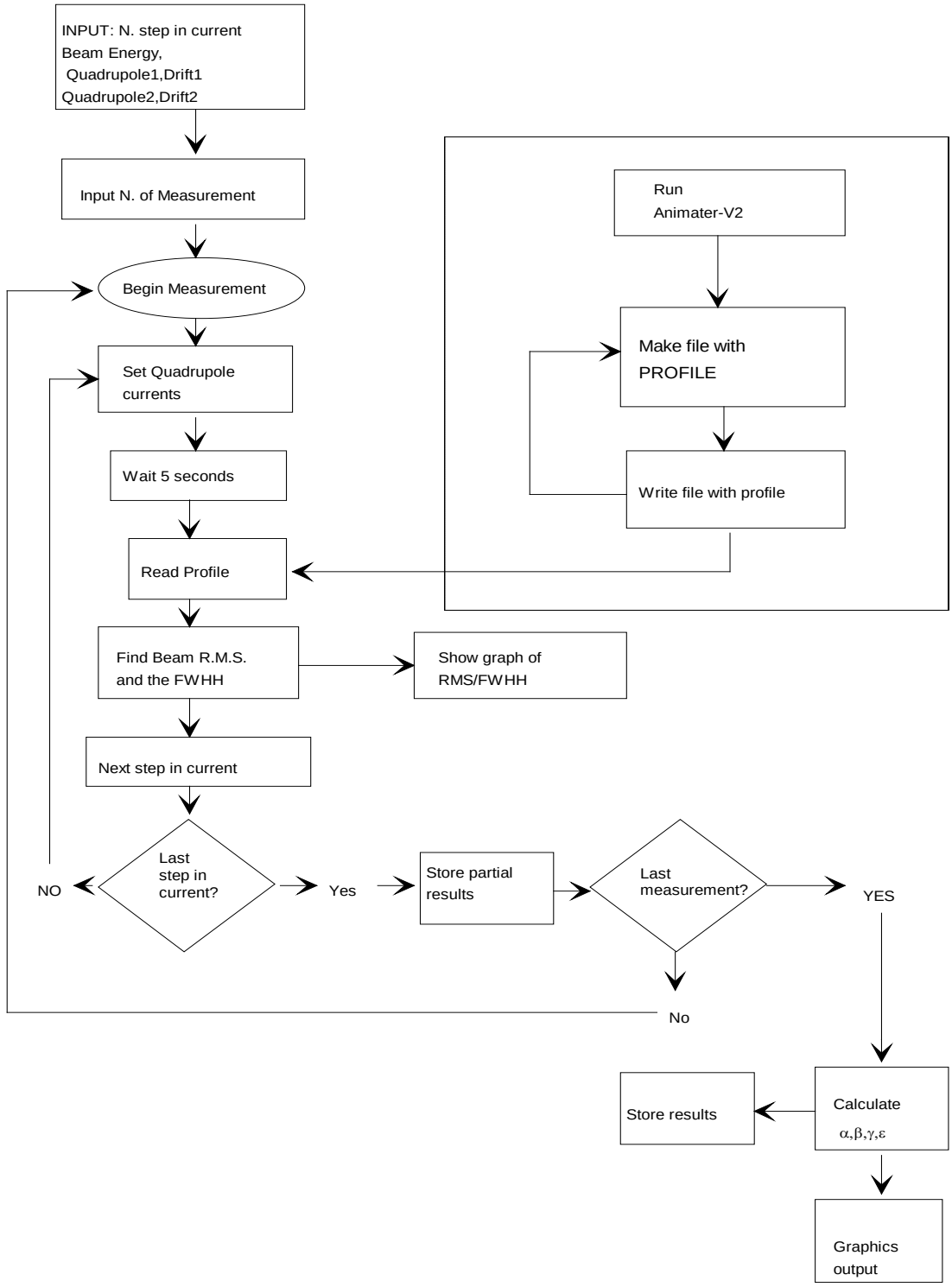

Figure 6.2 Flow chart of EASY

This flow chart describes how the program EASY works during the measure; all the inputs are given before the loop is started. The input of the profile comes from the camera software by a separate loop procedure made by a batch procedure with the commercial software Awlan. The program does not control all the parameters in the machine, but only the set up of quadrupoles. In figure 6.3 it's showed the graphic output of the program EASY during the measurement, as it appears to the operator.

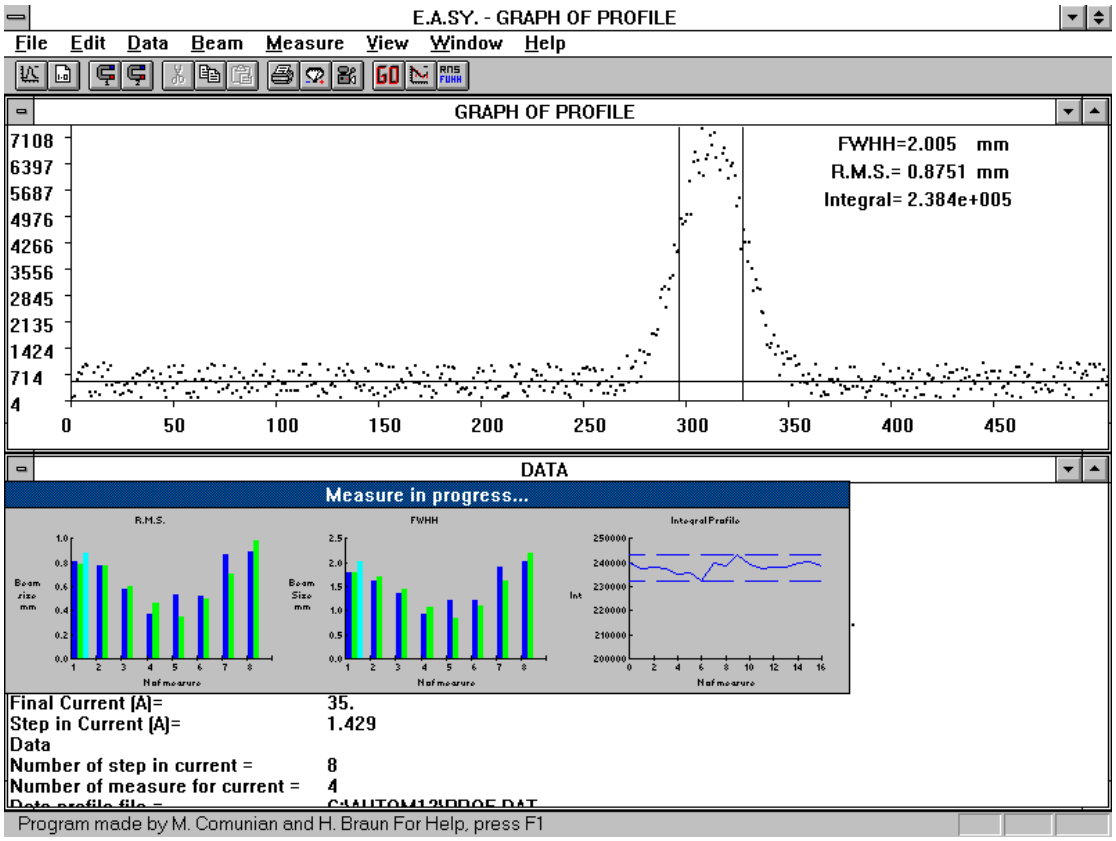

Figure 6.3 Look of the program E.A.SY. during the measurement process

In figure 6.4 it's reported the final result of the measurement as it appears to the operator.

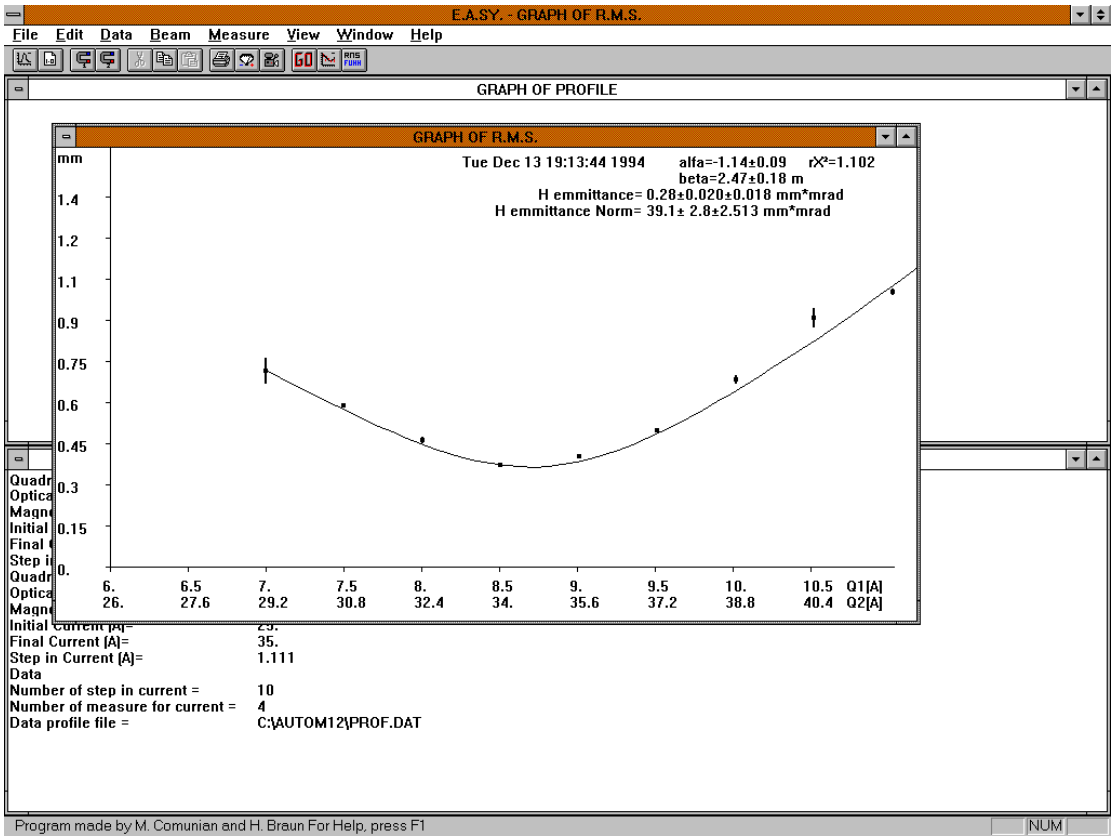

Figure 6.4 Look of the program E.A.SY. at the end of measurement

7. EMITTANCE MEASUREMENT RESULTS AND COMPARISON WITH THE PARMELA SIMULATIONS

7.1 Introduction

We have done emittance measurements in CTF from October to November 1994 in the run No. 2[xviii] and from November to December 1994 in the run No. 3[xix]. We have also done simulations of part of the CTF line with the program PARMELA[xx] in order to compare the theorical results with the experimental ones. The program PARMELA, "Phase And Radial Motion in Electron Linacs" is a versatile multi-particle code in which the beam, represented by a collection of particles, may be trasformed through a linac and/or transport system specifed by the user. It's also able to treat the space-charge forces properly.

The CTF line simulated in PARMELA is shown in figure 7.1, It is not necessary to simulate all the line, because we assume that the emittance is constant in the acceleration structure LAS. The space charge forces have a big effect on the emittance, at low momentum, so we take in account this effect in the simulated line.

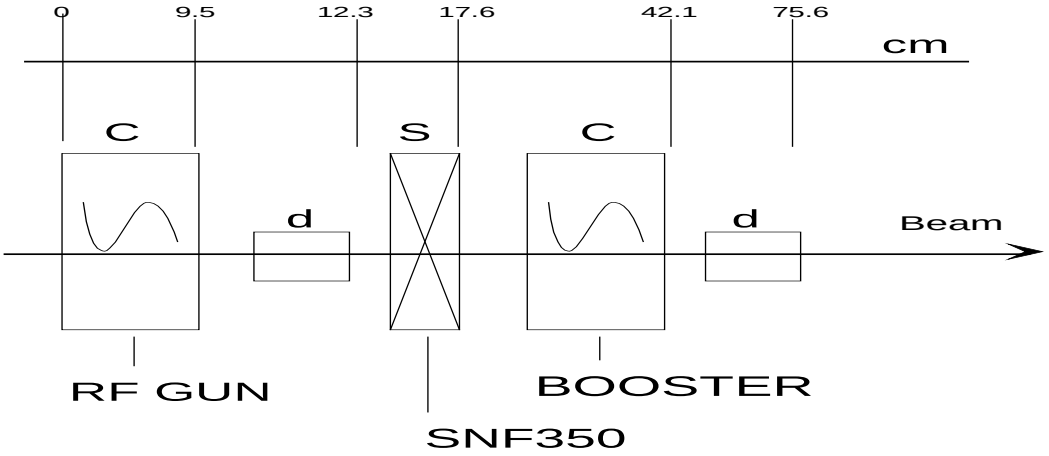

Figure 7.1 Line simulated in PARMELA

The main parameters used in these simulations are reported in table 7.1

Table 7.1 Parameters in the simulations with PARMELA

Eletric field in the GUN	100 MV/m
Eletric field in the BOOSTER	70 MV/m
Gun Frequency	2998.55 MHz
Solenoid SNF350	2300 Gauss
Phase in the GUN	30 deg.
Spot size	2.4 and 4.4 mm (σ)
Input Charge	from 0 to 20 nC
Pulse lenght	3 ps (σ)
Number of macro-particles	801

The results obtained are showed in table 7.2 and figure 7.2:

Table 7.2 Results of the simulations

Input charge [nC]	Emittance Normalized [mm*mrad]	Laser spot size [mm]	Final charge [nC]	Transmission []
0.0	16	4.4	0	1.0
2.5	26	4.4	2.5	1.0

5.0	39	4.4	5.0	0.99
7.5	51	4.4	7.4	0.98
10	60	4.4	9.7	0.97
15	73	4.4	13	0.89
20	81	4.4	16	0.80
0.0	4.6	2.4	0.0	1.0
2.5	21	2.4	2.5	0.99
5.0	28	2.4	4.8	0.95
7.5	37	2.4	6.8	0.91
10	43	2.4	8.6	0.86
15	49	2.4	11	0.72
20	53	2.4	12	0.60

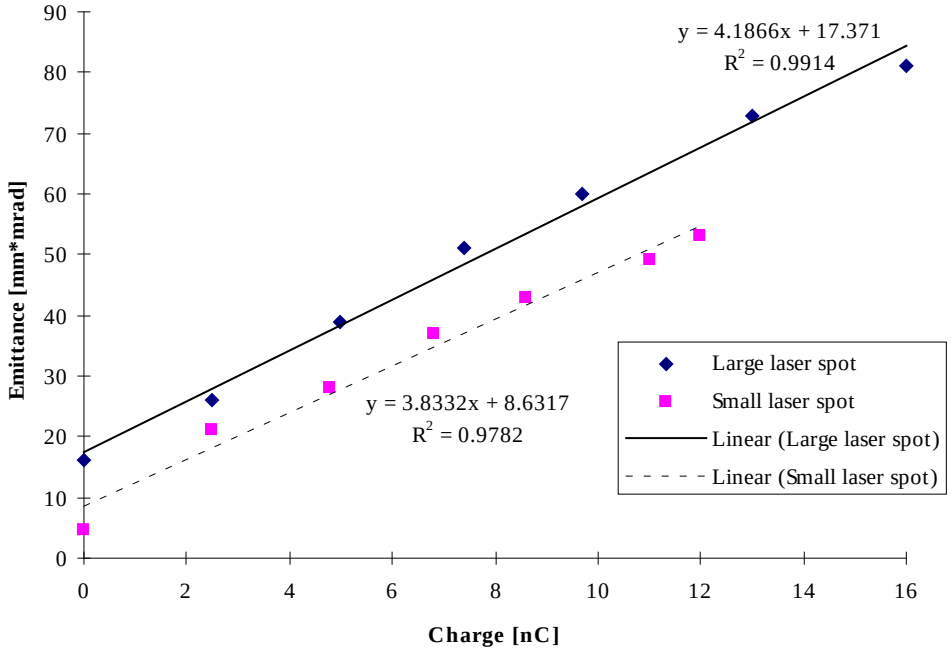

Figure 7.2 Emittance as function of final charge simulated by PARMELA

The figure 7.2 shows that the behaviour of the curve is almost linear, i.e. the emittance grows with the charge in linear way.

With a large spot size of the laser that hits the photocathode the emittance is larger than the emittance for small spot size.

7.2 Accuracy of simulations

The precision of the simulations done is related to our capacity to describe the physical phenomena that occour in reality, for example: space-charge and wake-fields effects. We had considered the space charge effect but not the wake-fields. Another aspect of simulations are the numerical parameters: for example what is the best number of particles to use in simulations?

For check the stability of the results we have done a statistical study: we have used twenty times the same input file and we have produced twenty different output results by the different random generator of the particle distributions. In figure 7.3 is reported the relative error on the emittance, obtained by the standar deviation (σ) divided by the emittance, as function of the number of particles used in the simulations. This shows that the precision of PARMELA goes almost like the square-root of the number of particles used.

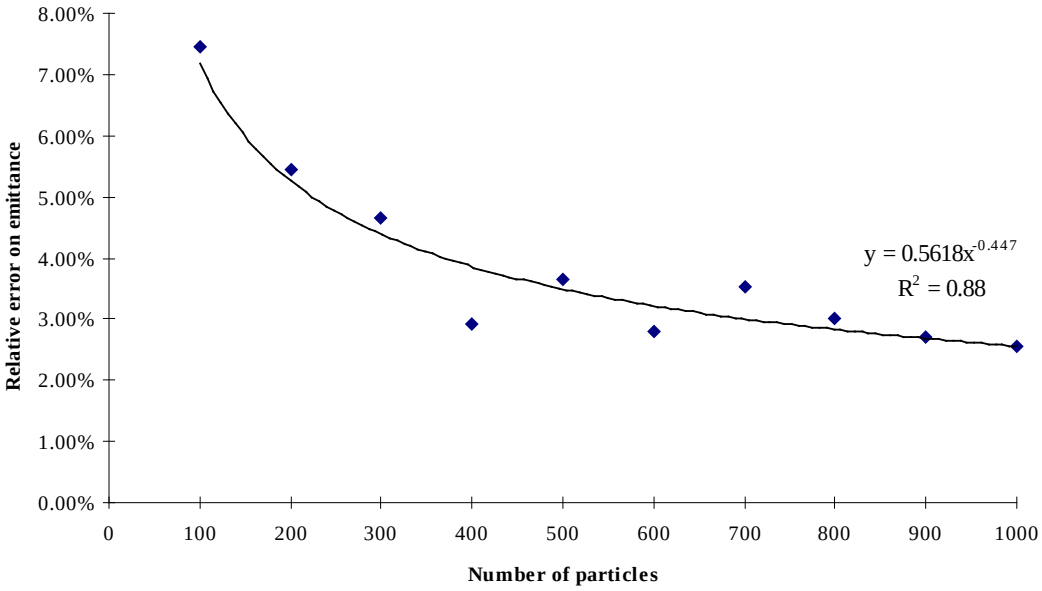

Figure 7.3 Precision of PARMELA

Figure 7.3 shows that is important to pass the knee zone, from 100 macro-particles to 400 macro-particles, to increase the precision of the simulations we have to use more than 500 macro-particles to minimize the effect linked to the number of macro-particles. We have studied also these effects with the space charge at 5 nC. The result is shown in figure 7.4 for the line shown in figure 7.1 and in this case the emittance it's almost constant. For a more realistic line with the two solenoid and quadrupoles and the accelerating section, see figure 2.1, the result is not more stable as shown in figure 7.5, the use of this line for the simulations is very time consuming.

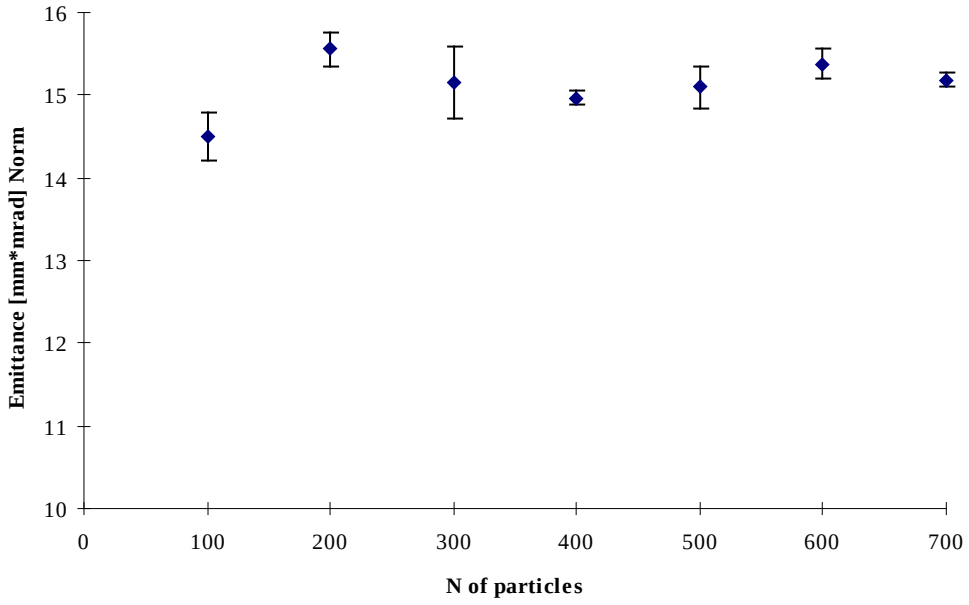

Figure 7.4 Emittance at 5 nC as function of the number of particles

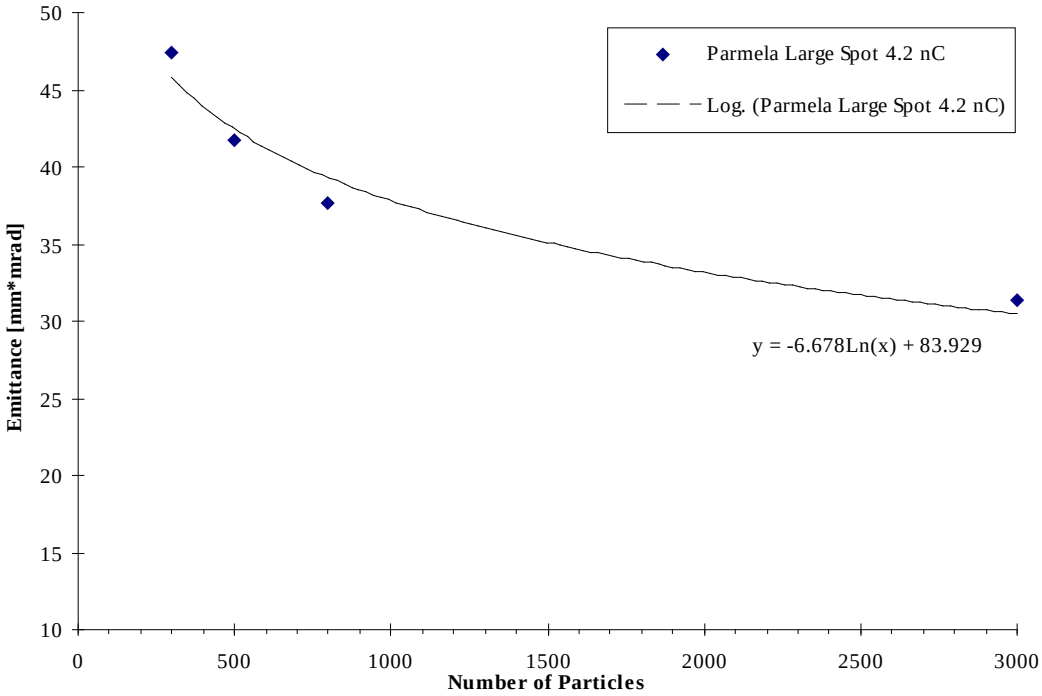

Figure 7.5 Emittance as function of number of particles

7.3 Errors in the measurement process

What we direct measure is the beam profile for different settings of the quadrupoles.

In the measurement process of the emittance the beam width measurement has a certain error due to beam instability and due to the precision of the reading the beam profile in the streak camera. Typically we repeat the quadrupoles scan four times, for to compute the errors associate to the beam profile, giving typically a relative error of 2% for the measurement of the R.M.S. values of the profile, formula 5.2, and 4% for the measurement of F.W.H.H. The details of the results are reported in figure 7.6.

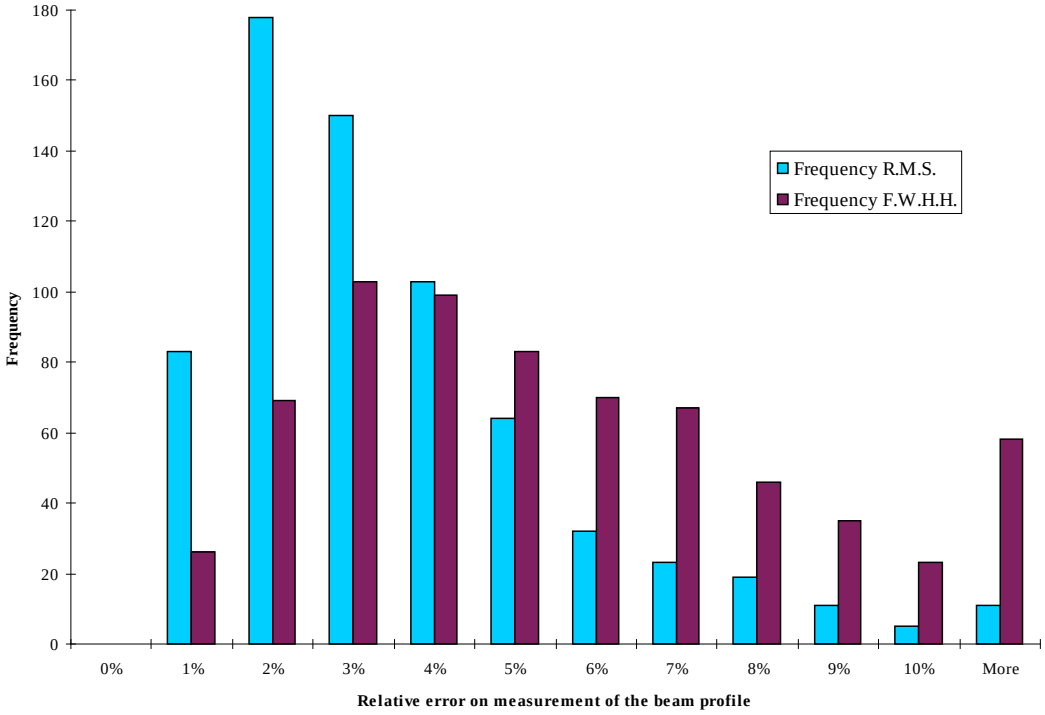

Figure 7.6 Frequency of the errors in measure of the beam profile

We have observed a smaller relative errors for the measure of the R.M.S. profile than for the measure of F.W.H.H profile.

The error on the measured normalized emittance is given by the propagation of the errors in the measurement of the beam profile, from the error in momentum (we assume a constant relative error of 3%) and from the errors calculated in the fitting routines (formulae 4.30-4.32). So the final result in the relative total error of measured normalized emittance R.M.S. is typically around 10%. (Figure 7.7)

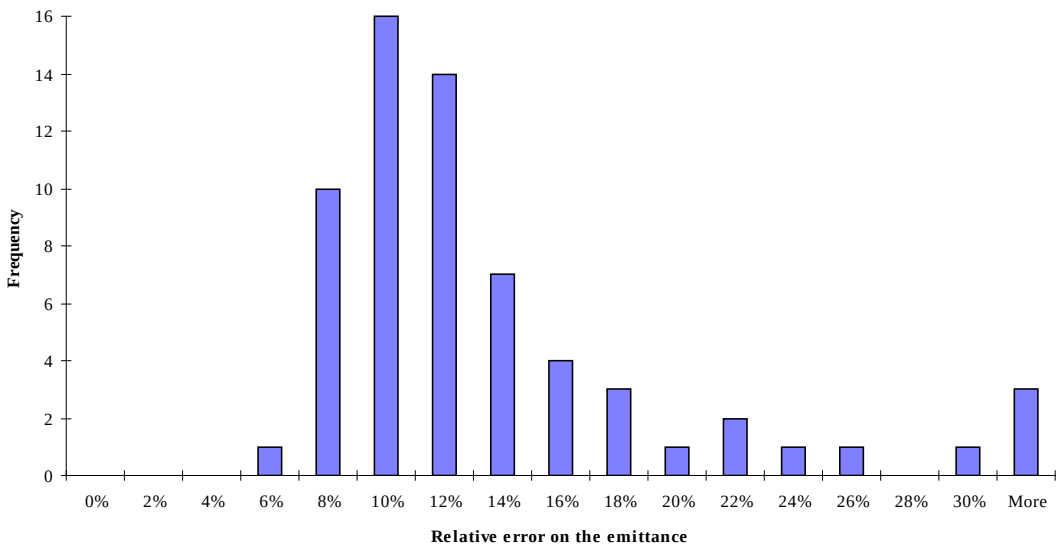

Figure 7.7 Relative error on the normalized emittance R.M.S.

We have also measured the Twiss parameters (α,β,γ), that define the optics of the beam, with errors around 7%, as shown in figure 7.8, the frequency gives how many measure we did with that error.

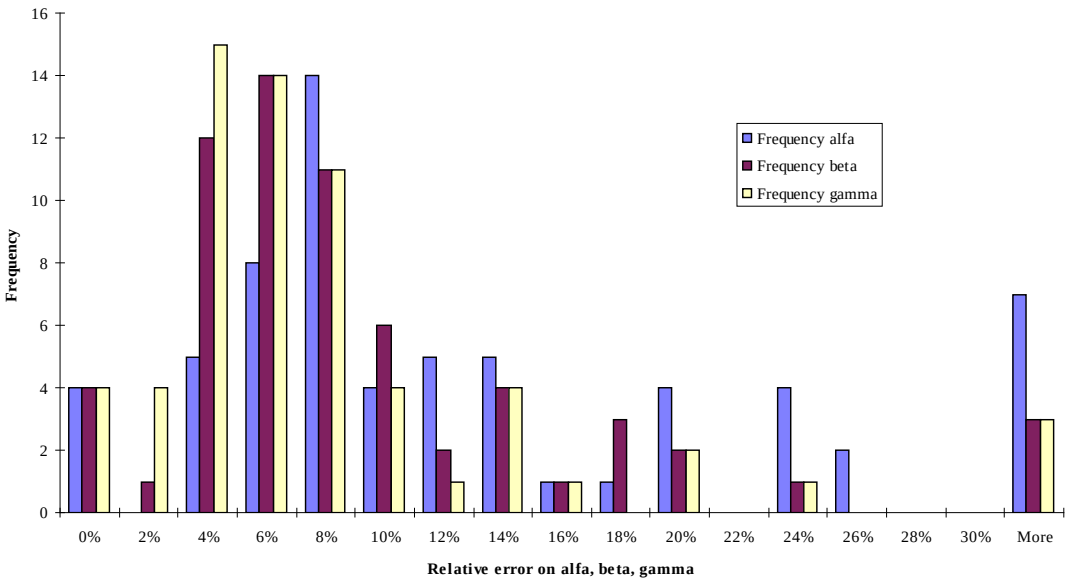

Figure 7.8 Relative errors on Twiss parameters

We observed a correlation between the absolute value of the Twiss parameter α and the relative error on the normalized emittance, i.e. when we did measurement with an optics producing a high value of α, the errors measured on the normalized emittance were larger than in the other measurement with a value of α near to zero. This fact is shown in figure 7.9.

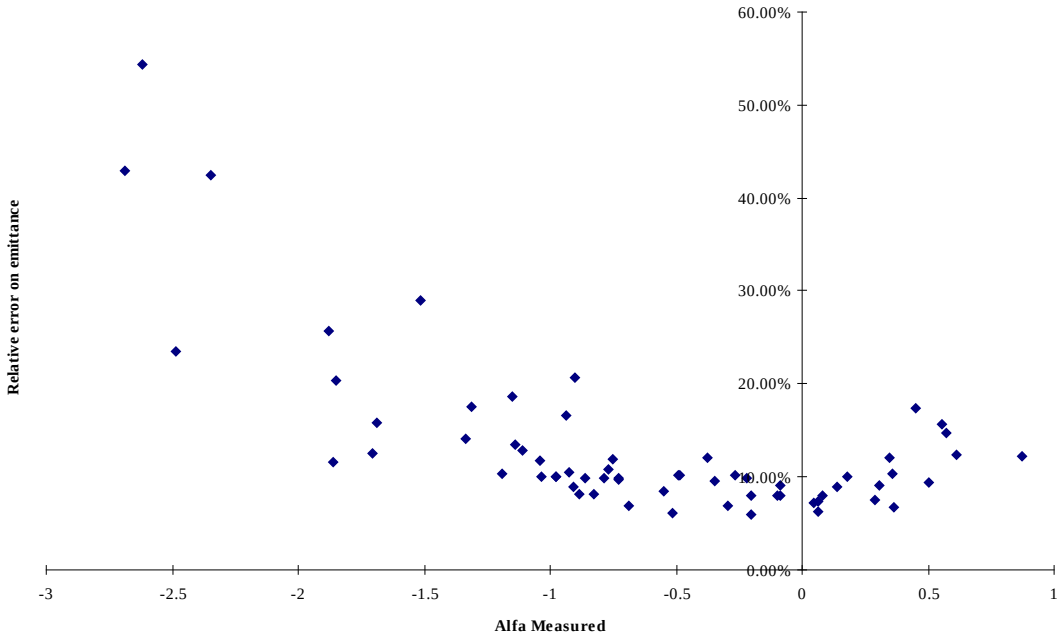

Figure 7.9 Correlations between α and the error on the measured emittance.

We have observed correlation only for this parameter, for β and γ there is not correlation between the value and the errors on the ε_{RMS} . A possible physical meaning of this is that when α is "big" we have a converging (or diverging) beam, there is then a strong correlations between the *x* and the *x'* variables and we are therefore less "sensible" in the beam profile position.

7.4 Measurement results

Table 7.3 are reports the measurement results of the emittance R.M.S. The phase out the gun for this measurement is 30 deg. usually.

Table 7.3 Results of the measurement

Date/time of the measure	**Charge**	**Laser spot size radius (error ± 0.5 mm)**	**Horizontal normalized Emittance R.M.S.**	**Total error on the emittance R.M.S.**	**Riduced χ^2 of the fitting**
Time	[nC]	[mm]	[mm*mrad]	[mm*mrad]	
Oct/17/94 18:14:02	1.2	5	29.3	4	0.5
Oct/17/94 19:05:10	2.7	5	41.9	4	0.3
Oct/17/94 19:33:28	5.7	5	69.1	6	0.9
Oct/20/94 12:54:44	1.8	5	34.9	3	5
Oct/20/94 13:34:42	5.1	5	54.8	6	0.7
Oct/20/94 15:41:20	9.0	5	89.9	15	0.1
Oct/21/94 17:23:48	16	5	61.6	4	0.8
Oct/21/94 17:40:40	16	5	117.5	11	4
Oct/21/94 18:43:20	20	5	86.4	10	16

Date/time of the measure	**Charge**	**Laser spot size radius (error ± 0.5 mm)**	**Horizontal normalized Emittance R.M.S.**	**Total error on the emittance R.M.S.**	**Riduced χ^2 of the fitting**
Time	[nC]	[mm]	[mm*mrad]	[mm*mrad]	
Oct/21/94 19:01:10	21	5	144.1	30	0.4
Nov/09/94 15:07:00	6.2	5	75.2	22	0.4
Nov/09/94 16:27:14	2.4	2.5	37.8	7	0.2
Nov/09/94 17:29:50	2.1	2.5	29.2	3	0.9
Nov/09/94 18:09:50	1.2	2.5	27.2	3	0.3
Nov/09/94 18:41:28	0.9	2.5	21.9	2	0.6
Nov/09/94 19:02:44	1.1	2.5	33.3	5	0.2
Nov/15/94 15:20:48	1.0	2.5	41.1	7	0.8
Nov/15/94 16:07:02	3.2	2.5	81.7	20	0.4
Nov/15/94 16:24:20	1.9	2.5	79.5	34	0.6
Nov/22/94 16:55:34	1.2	5	71.6	11	0.5
Nov/22/94 17:37:04	1.2	5	44.8 Vertical ε	5	0.3
Nov/22/94 18:01:56	1.2	5	48.0 Vertical ε	5	0.5
Nov/22/94 18:21:30	1.2	5	67.2	8	0.6
Nov/23/94 14:51:14	1.2	5	53.8 Phase=45 deg	6	0.6
Nov/23/94 15:09:36	1.2	5	51.6 Vertical ε Phase=45 deg	9	0.1
Nov/23/94 16:41:20	1.0	5	63.3 Phase=30 deg	8	0.4
Nov/23/94 16:57:44	1.0	5	42.2 Vertical ε Phase=30 deg	4	0.7
Nov/23/94 17:26:38	1.0	5	51.7 Phase=60 deg	4	0.4
Nov/23/94 18:19:48	1.0	5	44.8 Vertical ε Phase=60 deg	19	0.3
Nov/23/94	1.1	5	67.8 Vertical ε Phase=60	12	1.4

Date/time of the measure	Charge	Laser spot size radius (error ± 0.5 mm)	Horizontal normalized Emittance R.M.S.	Total error on the emittance R.M.S.	Riduced χ^2 of the fitting
Time	[nC]	[mm]	[mm*mrad]	[mm*mrad]	
19:13:32			deg		
Dec/13/94 16:40:42	4.2	5	46.3	6	0.3
Dec/13/94 17:15:56	2.3	5	39.9	6	0.3
Dec/13/94 18:33:38	2.3	5	36.3	4	1.8
Dec/13/94 19:13:44	2.3	5	39.1	6	1.1
Dec/14/94 16:28:16	4.2	2.5	146.4	16	0.3
Dec/14/94 16:59:12	0.7	2.5	22.3	2	0.7
Dec/14/94 17:27:02	1.6	2.5	38.0	4	0.7
Dec/14/94 17:51:58	2.2	2.5	75.2	8	0.8

In figure 7.10 we have reported the horizontal emittance as function of charge for all the measurement done, the trendline is almost linear.

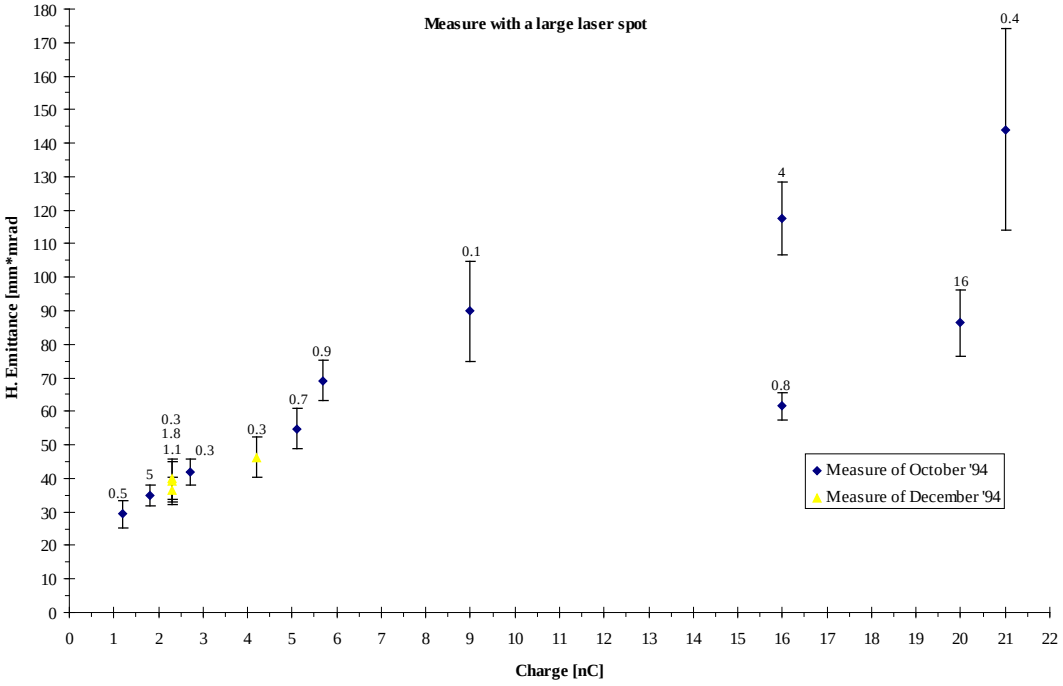

Figure 7.10 H. Emittance measured with large spot size

In figure 7.10 is reported the emittance measured with the small size in the laser spot, in this case there is not a clear trendline in the measure.

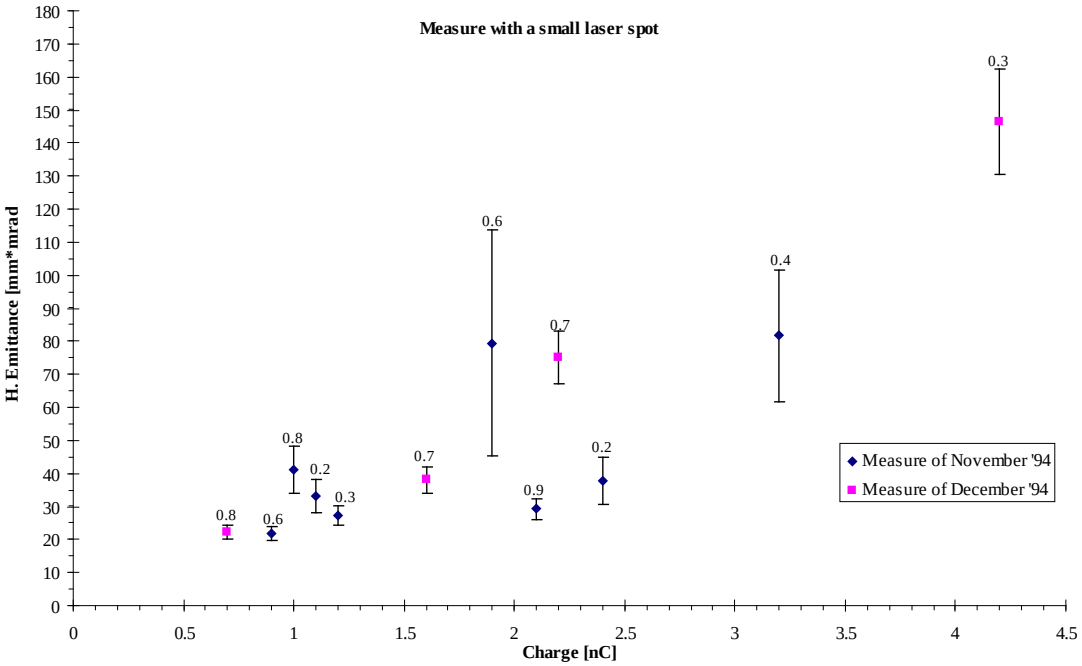

Figure 7.11 H. emittance measured with small spot size

We have done also measurement of the emittance as function of the phase in the gun for almost the same charge (~ 1 nC), the result is shown in figure 7.12. The emittance is not the same for the horizontal and vertical plane and there is not strong correlation with the phase in the gun.

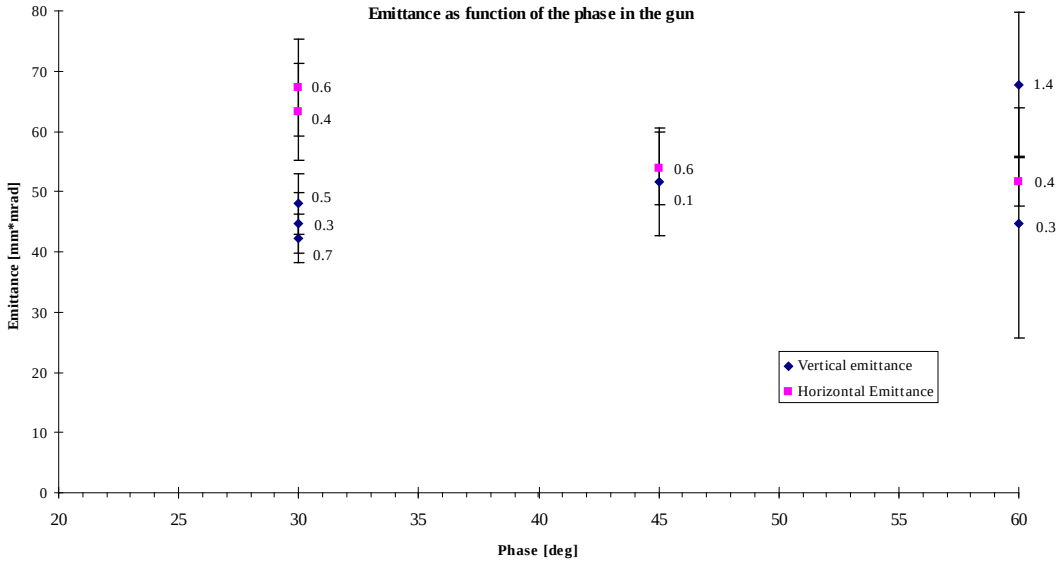

Figure 7.12 Emittance as function of the phase in the gun

7.5 Agreement between measurement and simulations

In figure 7.13 and 7.14 the measured emittance and the simulations done with PARMELA with large and small spot size are overlapped.

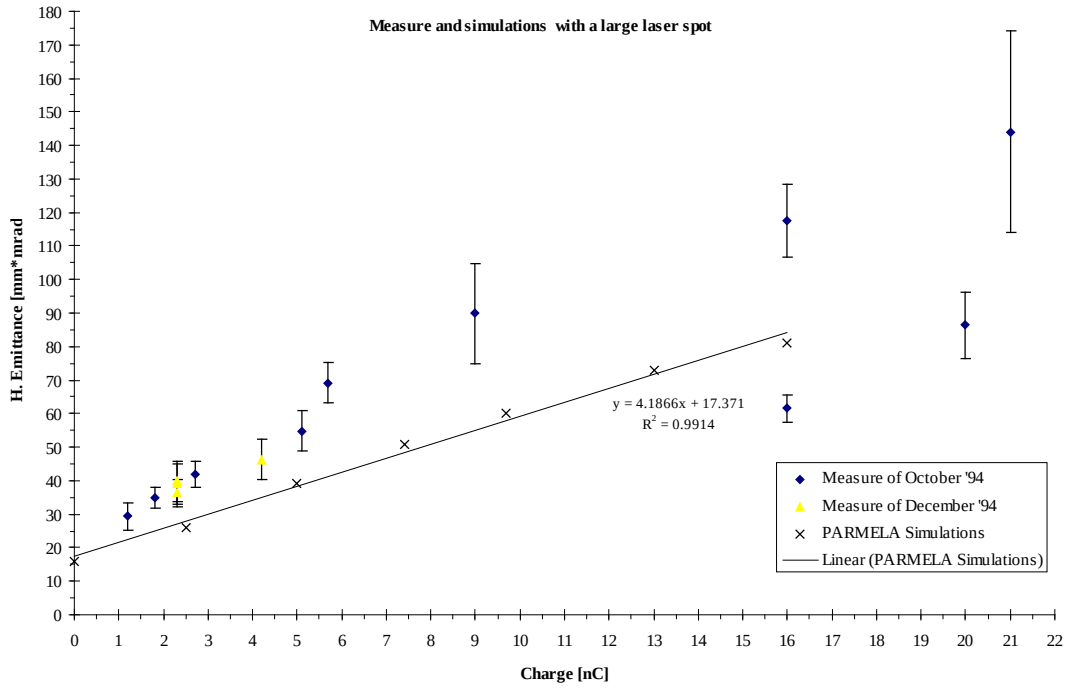

Figure 7.13 Measurements and simulations for large spot

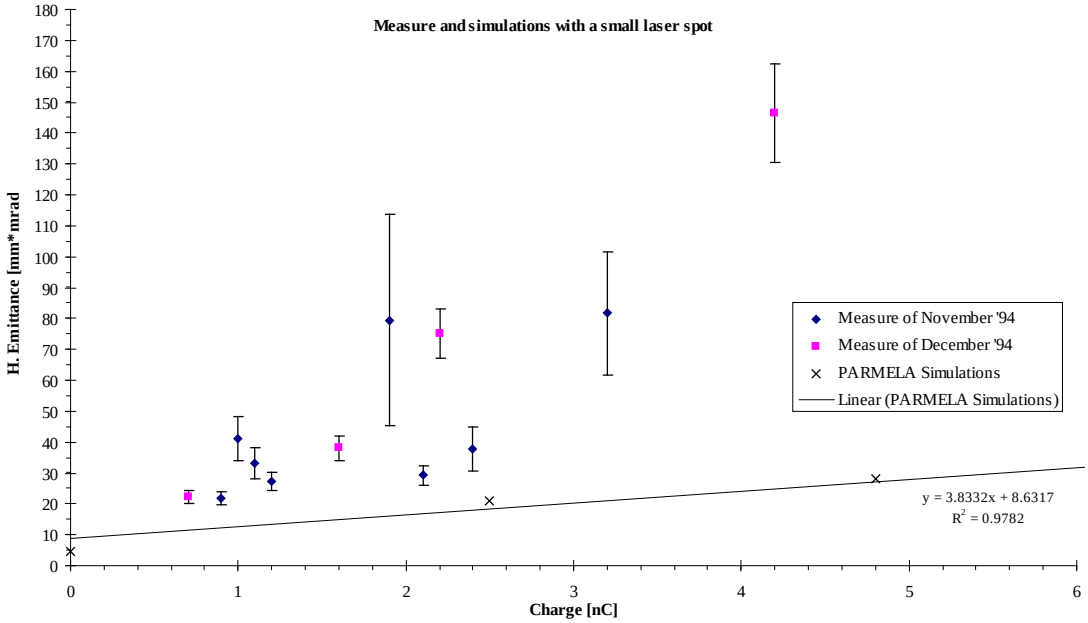

Figure 7.14 Measurements and simulations for small spot

These two graphs show that we had obtained a good agreement for the large spot size of the beam (~ 5 mm) but a bad one for the small spot size, more than a factor two of the difference.

[i] W. Schnell, The CERN study of a linear collider in the TeV range, CERN-SL/91-49.

[ii] P.J. Bryant, A brief history and review of accelerators, CERN ACCELERATOR SCHOOL 1992.
[iii] B. Autin et al., CLIC drive beam generation - a feasibility study, 1994 EPAC, London.
[iv] C. Fischer, Coping with alignment tolerances on CLIC components in the 10 μm range, CERN-SL/94-70.
[v] G. Guignard, Beam emittance preservation in linear colliders, CERN-SL/94-81 (AP).
[vi] L. Thorndahl, Efficiencies of 30 GHz power generation for CLIC, CLIC NOTE 259.
[vii] Y. Baconnier et al., A CLIC injector test facility, CLIC NOTE 65.
[viii] R. Bossart et al., Performances obtained with the CERN linear collider test facility (CTF), CERN-PS/94-17 (LP).
[ix] H. Braun, Parameter list of CTF, CERN-PS/93-23 (tech.) (LP).
[x] J. Buon, Beam phase space and emittance, CERN ACCELERATOR SCHOOL, 1992.
[xi] W. R. Leo, Techniques for nuclear and partilce physics experiments, Springer-Verlag, 1987.
[xii] H. Braun et al., The CTF run n. 3 -1994 results and comments, NOTE PS/LP (INFO) 95-01.
[xiii] S. Battisti, Measurement of the short bunch length in the CTF, CERN/PS 93-34 (BD).
[xiv] H. Braun et al., Beam dynamics for CTF, CLIC NOTE 243.
[xv] J.C. Thomi, La measure de profils longitudinaux de faisceaux d'electrons, NOTE PS/BD 93-03.
[xvi] D. Blechschmidt and D.J. Warner, Parameters of the LEP injector linacs, CERN/PS 88-07 (LPI).
[xvii] M. Comunian, The CTF beam emittance: measurement and computations, CERN PS/LP NOTE 94-57 (min.).
[xviii] J.H.B. Madsen et al., The CTF run no. 2 results and comments, CERN PS/LP NOTE 94-45.
[xix] J.H.B. Madsen et al., The CTF run no. 3 results and comments, CERN PS/LP NOTE 95-01.
[xx] B. Mouton, The PARMELA program, LAL/SERA/ 93-455.